

American Institute of Steel Construction  
www.aisc.org  
One East Wacker Drive Suite 700  
Chicago, IL 60601  
312.670.2400

September 15, 2014

Amit M. Kanvinde  
University of California - Davis  
2001, ENGR III  
Dept. of Civil & Env. Engineering  
Davis, CA 95616

RE: EJ Paper 2013-24 Rev.

Dear Professor Kanvinde,

This letter will confirm our agreement regarding the American Institute of Steel Construction ("AISC") use of your paper entitled "Seismic Response of Partial Joint Penetration Welded Column Splices in Moment Resisting Frames" in the *Engineering Journal*.

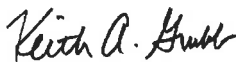
You confirm, and AISC acknowledges, your ownership of the copyright to the Paper. You acknowledge and agree that AISC intends to include the Paper in a future issue of the *Engineering Journal* and that AISC will have all right, title, and interest in the *Journal* and the copyright to the *Journal*.

You also acknowledge and agree AISC shall have the right to use the Paper for any additional purposes, including publication in other compilations or singly, or in online database files. Therefore, you hereby grant AISC a perpetual, royalty-free, nonexclusive license to use, copy, display, and/or distribute the *Engineering Journal* Paper for any purposes and in any medium, including videotape presentations.

Please sign and return this letter to indicate your agreement with the foregoing.

We are pleased you have agreed to publish your paper in the *Engineering Journal*.

Sincerely,



Keith A. Grubb  
Editor - *Engineering Journal*  
American Institute of Steel Construction

AGREED:

  
\_\_\_\_\_  
Author's Signature

9/15/2014  
\_\_\_\_\_  
Date



There's always a solution in steel.

# Seismic Response of Partial Joint Penetration Welded Column Splices in Moment Resisting Frames

SEAN M. SHAW<sup>1</sup>, KIMBERLY STILLMAKER<sup>2</sup>, AND AMIT M. KANVINDE<sup>3#</sup>

## ABSTRACT

Current standards require that welded column splice connections in Special or Intermediate Moment Resisting Frames (SMRFs or IMRFs) feature Complete Joint Penetration (CJP) groove welds to develop the full flexural strength of the column. In contrast to PJP welds, CJP welds are often costly, requiring additional material, inspection and back-gouging or backing-bar removal to ensure complete penetration. However, unlike welded beam column connections which fractured in the 1994 Northridge Earthquake, column splices have modest deformation demands. This suggests that perhaps with modern, toughness-rated weld filler materials and welding practice, PJP welded splices may offer acceptable performance under seismic loads. Motivated by these observations, a study featuring five full-scale tests on PJP-welded column splices is presented to examine their feasibility for use in IMRFs or SMRFs in seismic environments. The test matrix investigates a range of parameters including column sizes (consistent with use in 4, 9 and 20 story buildings) as well as variations in connection details (single and double-beveled, welded and unwelded webs, presence of a weld access hole). All specimens utilized columns with specified yield strength 50 ksi for the columns and ultimate strength 70 ksi for the weld electrode. The specimens were loaded cyclically in a three-point bend configuration such that the splice was subjected to demands consistent with those in severe earthquakes; a loading protocol was developed specifically for this purpose based on Nonlinear Time History simulations. All the full-scale specimens exhibited excellent performance, such that the splices exceeded the moment capacity of the smaller connected column. The full scale data is complemented by a series of ancillary tests such that the results may be interpreted with respect to measured, rather than specified material properties. A series of Finite Element (FE) fracture mechanics simulations is also presented to assist with the generalization of test results. The FE simulations indicate that for the tested connections, the toughness demands are below the minimum expected toughness suggesting that details similar to the ones tested in the study may be suitable for general use in the field. A synthesis of the test and simulation data is encouraging from the perspective of adoption of PJP welded splices in IMRFs and SMRFs in seismic regions. Limitations of the research are outlined, along with discussion of future work to develop further support for the use of PJP welded splices in moment frames.

---

<sup>1</sup> Design Engineer, Buehler and Buehler Structural Engineers, Sacramento, CA, 95811.

<sup>2</sup> Graduate Research Assistant, Department of Civil and Environmental Engineering, University of California, Davis CA 95616.

<sup>3</sup> Associate Professor, Department of Civil and Environmental Engineering, University of California, Davis, CA 95616, Email: kanvinde@ucdavis.edu

# Corresponding Author

31 **INTRODUCTION**

32 The 1994 Northridge earthquake revealed the susceptibility of Welded Beam to Column (WBC) connections to  
33 fracture. Numerous studies associated with the SAC Steel Project (SAC, 1996) such as Engelhardt and Sabol (1994)  
34 exhaustively examined the factors responsible for these fractures and developed recommendations for new  
35 construction as well as retrofit (FEMA, 2000). By and large, these studies concur that the WBC fractures may be  
36 attributed to a combination of (1) low toughness in the base and/or weld material (2) poor detailing practice; e.g., the  
37 use of backing bars and weld runoff tabs, which produced flaws or cracks in highly stressed regions of the flanges,  
38 and (3) connection configurations which did not account for unanticipated stress distributions, e.g. the amplification  
39 of shear and longitudinal stress in the flanges due to inadequate participation of the web connection. Informed by  
40 these investigations, subsequent design standards (e.g. AISC 341-10, 2010) mandate stringent requirements for  
41 material toughness (based on Charpy V Notch testing of base and weld material), detailing, and guidelines for  
42 connection design and inspection. As a result, the fracture risk in WBC connections has been mitigated to a large  
43 extent.

44  
45 The post-Northridge research discussed above primarily addressed WBC connections, because a vast majority of the  
46 fractures during the Northridge earthquake were observed in these connections. However, the broader findings  
47 regarding the fracture-susceptibility of details with effect of sharp flaws and brittle materials resulted in updated  
48 design requirements for other connections as well. These include column splice connections, which are commonly  
49 used in moment frames due to one or more of the following reasons (1) column sections are typically transitioned to  
50 account for changes in loading over the height of the building (2) the height of the building is greater than the length  
51 of the available section (3) shipping constraints and erection practices limit the length of the columns. To reflect the  
52 need for more stringent detailing requirements in these connections, the current edition of *The Seismic Provisions*  
53 (AISC 341-10, 2010) prescribes the following for Intermediate and Special Moment Resisting Frames (IMRFs and  
54 SMRFs): “Where welds are used to make the splice, they shall be complete-joint-penetration groove welds.”

55  
56 Figure 1a schematically illustrates a pre-Northridge column splice connection, whereas Figure 1b indicates a post-  
57 Northridge connection designed as per the improved guidelines outlined above. Referring to Figure 1, the main  
58 difference between the pre- and post-Northridge type connections is that the post-Northridge connections

59 incorporate Complete Joint Penetration (CJP) welds in the flanges and the webs (to develop the flexural strength of  
 60 the column by eliminating the crack-like flaw at the Unfused Weld Root - UWR), whereas the pre-Northridge  
 61 connections used Partial Joint Penetration (PJP) welds, with weld penetration (or effective throat) in the range of 40-  
 62 60% of the flange thickness. The newer splice details with the CJP welds are significantly more expensive to  
 63 construct for several reasons. First, more weld material must be used, since full penetration is required; the volume  
 64 of weld material is nonlinearly proportional to the extent of penetration. Second, the use of additional weld material  
 65 requires a greater number of weld passes, requiring surface preparation and cleaning between each pass. Third, and  
 66 perhaps most important, complete penetration typically requires back-gouging and welding the material near the  
 67 weld root from the opposite side, such that no part of the connection remains un-fused. Alternative processes, such  
 68 as using a backing-bar are possible as well, although sometimes undesirable due to stability concerns. Finally,  
 69 demand critical CJP welds require rigorous inspection protocols. It is especially inconvenient and costly to conduct  
 70 these processes since the splices are always field-welded, often several stories above the ground.

71

72

73

74

75

76

77

78

79

80

81

82

83

84

85

86

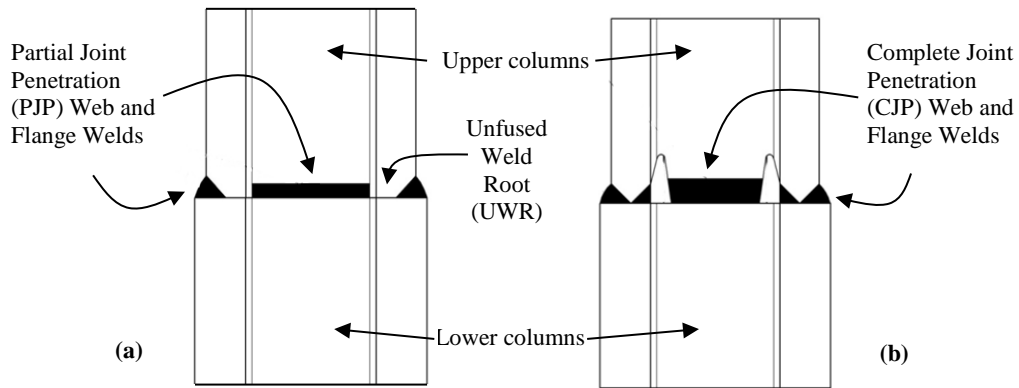


**Figure 1** – Column splice construction practice (a) Pre-Northridge and (b) Post-Northridge.  
 Erection plates on web not shown for clarity

In light of the above observations, it is also relevant to reference other aspects of the post-Northridge connections as well as recent research on other welded connections. Specifically, the current version of the *Seismic Provisions* (AISC 341-10, 2010) identifies the welds in the splices as “demand critical” welds, requiring that the weld filler metals must meet minimum toughness requirements (i.e. minimum Charpy V Notch energy of 20 ft-lb at 0°F and additionally, a CVN energy of 40 ft-lb at 70°F from heat input envelope testing). This is significantly higher as compared to the weld materials used in pre-Northridge connections. For comparison, the E70T-4 weld filler metal

87 typically used in pre-Northridge details exhibited Charpy V Notch energy values in the range of 5-10 ft-lb at 20°F  
88 (Kaufmann and Fisher, 1995). Moreover, the *Seismic Provisions* (AISC 341-10, 2010) also require the column  
89 splice to be located either 4 feet away from the ends of the column, or at the center of the column if the story height  
90 is less than 8 feet. It is considered unlikely that this location (and hence the splice) will be subjected to high inelastic  
91 rotation demands, for the following reasons: (1) The Strong Column Weak Beam (SCWB) requirement encourages  
92 the development of plastic hinges in the beams, under first mode response (2) The absence of transverse load on the  
93 column implies that the peak moments are attained at the ends (rather than in the center) of the columns; in fact  
94 under first mode response which dominates most low- to mid-rise buildings, the bending moment near the center of  
95 the column approaches zero as the column bends in double curvature. Prior analytical research by Shen *et al.*, (2010)  
96 indicates that the splices are not subjected to significant inelastic action, even under extreme seismic events. The  
97 findings of this research are confirmed by similar simulations conducted as part of the current study (described in a  
98 subsequent section of this paper). Finally, recent research on other types of connections by the lead investigator of  
99 this study, e.g. Myers *et al.*, (2009), Gomez *et al.* (2010) and others (Dubina and Stratan, 2002), indicates that when  
100 high-toughness materials (similar to those required by post-Northridge design standards) are used, the presence of a  
101 flaw or crack-like stress raiser (produced, for example, due to the UWR) may be tolerated without brittle fracture.

102

103 When considered together, the above observations suggest that (1) inelastic deformation demands in splices may be  
104 relatively modest and (2) even if these demands are present, the use of appropriately designed PJP details may  
105 successfully mitigate fracture risk. This is important, considering the expense and inconvenience of constructing  
106 CJP welds in column splices. Motivated by these observations, this paper presents a series of full-scale tests on  
107 column splice connections welded with PJP welds and high-toughness weld filler metals. The main objective of the  
108 study is to investigate the seismic performance of these connections, and to examine their feasibility for use in  
109 SMRF/IMRF structures in highly seismic environments. The paper begins with a discussion of relevant literature in  
110 the area, with the objective of establishing context for the current study. This is followed by a discussion of a series  
111 of Nonlinear Time History (NTH) simulations that were conducted to characterize the demands in column splices  
112 and to develop a loading protocol for the full scale testing. The column splice tests (which feature Grade 50 base  
113 materials, and E70 weld electrodes) are then presented, along with analysis and discussion which also leverages

114 ancillary tests conducted to establish material constitutive and toughness properties. The paper concludes with a  
115 discussion of fracture mechanics analysis, which examines the potential for generalization of test results.

116

117

### LITERATURE REVIEW AND OBJECTIVES

118 Although guidelines for the design of column splice connections are stringent and similar to other connections such  
119 as WBC connections, research directly addressing column splice connections for seismic conditions has been  
120 relatively sparse. In fact, the only experimental study on fracture-critical welded column splices was conducted by  
121 Bruneau and Mahin (1991) prior to the Northridge earthquake. Other previous studies on column splices (Popov and  
122 Stephen, 1976; and Hayes, 1957) have examined the response of spliced columns in compression. The Bruneau and  
123 Mahin (1991) study featured two column splice specimens, which connected heavy rolled sections (W14×665  
124 connected to W14×500 and W14×426 connected to W14×370), with flanges in the thickness range of 2.6 – 4.5  
125 inches. The specimens were constructed to replicate erstwhile construction in terms of material properties, weld and  
126 member sizes, residual stresses as well as detailing practice and welding procedures. Of these two specimens, one  
127 featured PJP welds in the flanges with 50% penetration, whereas the other featured CJP welds with weld access  
128 holes. The specimens were subjected to cyclic loading under a four-point bend configuration, such that the splice  
129 region was subjected to pure flexure. As a consequence, the effect of shear was not considered. The prominent  
130 findings of this study were that (1) the CJP welded splice exhibited excellent performance sustaining moments  
131 greater than the cross-sectional strength of the smaller connected column (2) although the PJP welded splice failed  
132 in a brittle manner, it did so after the net-section strength of the connection (i.e. the strength based on the cross-  
133 sectional area, discounting the unfused root region) was reached. This implies that locally, the weld material had  
134 sufficient toughness to allow yielding over the entire weld ligament (i.e. connected portion), even if the  
135 corresponding strength was not sufficient to prevent brittle fracture of the connection when considered at the  
136 component scale.

137

138 The latter is an important observation in the context of the present study because weld and base materials used in the  
139 Bruneau and Mahin (1991) tests were not subject to minimum toughness requirements which were enforced after the  
140 Northridge earthquake and ensuing research. As outlined in the introduction, toughness of contemporaneously used  
141 weld filler metals (such as E70T-4) is significantly lower than what is currently required. Thus, the performance of

142 PJP connections in the Bruneau and Mahin (1991) study indicate the possibility of successfully using toughness  
143 rated filler materials with PJP weld details.

144

145 Nuttayasukul (2000) conducted fracture mechanics based finite element simulations of the Bruneau and Mahin  
146 (1991) tests, as well as additional parametric simulations of column splice details with PJP welds. The finite element  
147 study confirmed the internal stress distributions determined by Bruneau and Mahin (1991). The fracture mechanics  
148 simulations also suggest that despite the absence of a minimum specified toughness, pre-Northridge weld materials  
149 may have had sufficient toughness to develop the net-section strength of the PJP connection, if an adequate degree  
150 of effective throat thickness (> 50% of flange thickness) were provided.

151

152 Shen *et al.*, (2010) conducted a series of Nonlinear Time History (NTH) simulations to examine seismic demands in  
153 column splices. Given the absence of similar studies prior to this, the primary aim of the Shen *et al.*, (2010)  
154 investigation was to develop seminal understanding of the force and deformation demands in column splices such  
155 that the margin of safety provided by current design/detailing practice could be evaluated, with a possibility of  
156 lowering the stringency of detailing requirements. The NTH simulations were conducted for 4-, 9- and 20-story  
157 moment frame buildings subjected to a suite of 20 ground motions representative of the Southern California region.  
158 The simulations revealed that even under extreme ground motions (consistent with MCE or Maximum Considered  
159 Earthquake levels), the inelastic deformation demand in the splices is negligible, when interpreted at the macro-scale  
160 (or cross-sectional level). However, the force demands approach the capacity of the smaller connected column.  
161 Shen *et al.*, (2010) characterized the force demands in terms of a P-M Interaction Ratio ( $IR$ ), which reflects the  
162 combined effect of the axial tension and bending moment, such that  $IR = 1$  implies tensile yielding at the flange of  
163 the smaller (upper) connected column. This is because owing to the UWR, splice fracture is sensitive to a peak  
164 tensile stress in the flange of the connection. Consequently, the  $IR$  is an appropriate indicator of splice distress.  
165 Expectedly, the demands were highest (i.e. peak  $IR \approx 1.0$ ) for the 20-story building because of (1) higher  
166 overturning moments, increasing the axial tension in the exterior columns and (2) the pronounced participation of  
167 higher dynamic modes, resulting in single-curvature bending of some columns. The latter effect was dominant. For  
168 the 4-, and 9-story frames, the force demands were significantly lower (i.e. peak  $IR$ , computed over all the motions  
169 for the 4-story frame was in the range 0.35-0.8, whereas for the 9-story frame it was in the range of 0.5-0.9).

170 A synthesis of these three studies on column splices, along with other research (e.g. Myers *et al.*, 2009) that focused  
171 on the deformation capacity of other PJP welded connections (i.e. column base plates), yields the following  
172 observations –

- 173 1. The testing by Bruneau and Mahin (1991) and complementary FE simulations by Nuttayasukul (2000) suggest  
174 that even without the enforcement of current toughness requirements, pre-Northridge type PJP welds offered  
175 sufficient toughness to develop the net-section strength of the welded flanges, provided sufficient weld  
176 penetration was provided.
- 177 2. While column splices may be subjected to high force demands (approaching the capacity of the smaller  
178 connected column), the inelastic deformation demands are minimal or absent.
- 179 3. Other types of connections that incorporate PJP welds (such as base plate connections featuring notch tough  
180 material compliant with the *Seismic Provisions*), tested by Myers *et al.*, (2009) and more recently Gomez *et al.*,  
181 (2010) show excellent performance with the capacity to fully develop the column flanges in yielding.

182 Based on these observations, the specific objectives of the study presented in this paper are –

- 183 1. To experimentally examine the performance of various PJP-welded column splices under a test protocol  
184 representative of seismic loading.
- 185 2. To conduct a program of ancillary material tests and fracture mechanics analysis to examine the feasibility of  
186 these connections in steel moment frame construction in seismic regions.

187 The next section describes the Nonlinear Time History simulations conducted for assessment of demands in the  
188 splices and the loading protocol developed from these simulations.

189  
190  
191  
192

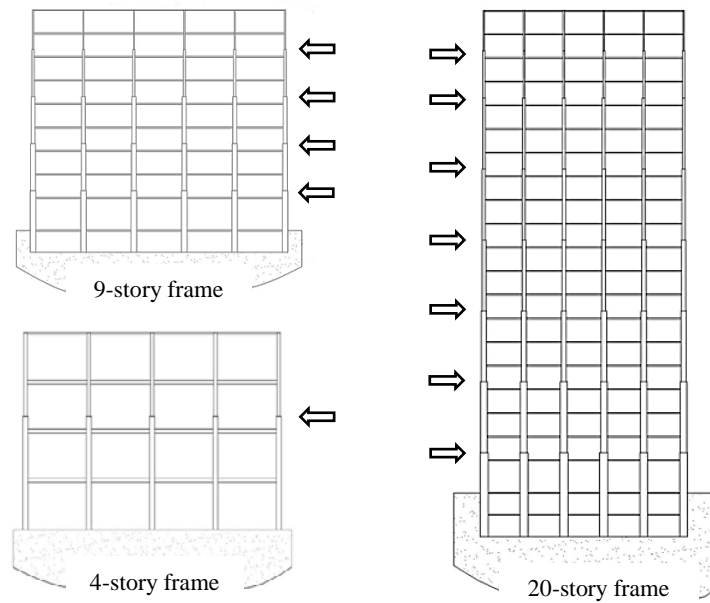
### **NONLINEAR TIME HISTORY SIMULATION, DEMAND CHARACTERIZATION AND DEVELOPMENT OF LOADING PROTOCOL**

193 An understanding of seismic demands in column splices in moment frames is critical for two reasons. First, it  
194 provides context for evaluating the vulnerability of splices that may be constructed using PJP welds. Second, and  
195 perhaps more important to this study, an analysis of the demands enables the development of a loading protocol for  
196 application to the full-scale splice specimens described in the next section. The development of such a protocol is  
197 necessary, because existing protocols for SMRF components (Gupta and Krawinkler, 1999) address seismic  
198 demands only in deformation-controlled components (such as beam-to-column connections). Column splices in  
199 SMRFs are primarily load (i.e. force and moment) controlled, because inelastic deformations are not expected at the



200 component level, albeit local yielding in the weld region is possible. Protocols for these types of components  
 201 (specifically splices) are not available; nor is it appropriate to adapt protocols developed for deformation controlled  
 202 components. Consequently, the large scale testing requires the development of loading histories that represent  
 203 seismic demands at the splice in a reasonable, yet conservative manner. A comprehensive program of Nonlinear  
 204 Time History (NTH) simulations was conducted, with the specific objective of assessing splice demands in the  
 205 context of developing a loading protocol. The NTH simulations conducted in this study are targeted specifically  
 206 towards the development of loading protocols. It is relevant to discuss here that previous NTH simulations targeted  
 207 towards the development of loading protocols (e.g. refer Gupta and Krawinkler, 1999) have employed ground  
 208 motions that are scaled such that they represent a target probability of exceedance, e.g. 10% in 50 years (i.e. a 10/50  
 209 hazard). Figure 2 indicates the buildings used for the NTH simulations used in this study, whereas subsequent  
 210 discussion addresses the NTH simulation and protocol development.

211  
212  
213  
214  
215  
216  
217  
218  
219  
220  
221



222 **Figure 2** – Schematic illustration of the three model buildings with arrows indicating spliced stories

223 1. Three generic frames (4-, 9- and 20- story) were used – see Figure 2. These are identical to the frames used by  
 224 Shen *et al.*, (2010), and are adapted from the SAC model buildings (Gupta and Krawinkler, 1999), with the  
 225 exception that the 3-story SAC model building was replaced by a 4-story building to accommodate the splice  
 226 (which is uncommon for shorter buildings). The frames have fundamental periods of 0.93, 1.75 and 2.33  
 227 seconds respectively. The frames were assumed to be constructed for a seismic environment (and typical gravity

228 loading) consistent with the Los Angeles, California region with assuming firm soil conditions (NEHRP site  
229 class D). Refer Shaw (2013) for more details regarding the building designs, Figure 2 shows the frames,  
230 including the locations of the splices (located 4 feet from the top surface of the beam in the lower story).

231 2. Each frame was subjected to a suite of 20 ground motions. These motions, developed during the SAC steel  
232 project (Somerville *et al.*, 1997) are titled LA21-LA40, and are based on recordings from the 1994 Northridge,  
233 1995 Kobe, 1989 Loma Prieta and the 1974 Tabas earthquake, in addition to simulated motions. The ground  
234 motions were scaled to match two spectra, consistent with the 10/50 and 2/50 hazard (as per ASCE 7-10) at a  
235 general location in the Los Angeles basin. Thus, a total of 40 motions ( $20 \times 2$  scaling levels) were used.

236 3. The simulations were conducted on the platform OpenSEES (2009) which has the capability to simulate several  
237 physical aspects of response. The specific modeling considerations included –

- 238 • The use of fiber sections for simulation of the beams and columns to represent axial-moment  
239 interaction and the spread of plasticity. The fiber sections utilized a bilinear steel material model with  
240 kinematic hardening. Material parameters were calibrated to match a comprehensive data set of plastic  
241 hinge response compiled previously by Lignos *et al.*, (2011). The calibrated values of the parameters  
242 are  $E = 29,000ksi$ ,  $F_y = 55ksi$  (to account for material overstrength with respect to specified  
243 strength) and the post-yield (i.e. hardening) slope 1.7% of the initial elastic modulus.
- 244 • Finite joint sizes were modeled. This is especially important since flexural demands at the splice are  
245 sensitive to its distance from the end of the column (at the beam face).
- 246 • Geometric nonlinearity, i.e.  $P - \delta$  and  $P - \Delta$  effects were modeled.

247  
248 Several variables were monitored during the NTH simulations. While the interstory drift and inelastic rotations are  
249 of interest, the time histories of longitudinal stress at the locations of the splices (specifically in the flange regions)  
250 are determined to be the most critical in the context of this study. This is because the primary concern with respect  
251 to the PJP welded splices is fracture at the UWR (see Figure 1 introduced previously). This type of fracture may be  
252 considered stress-controlled, since the inelastic deformation (at the splice component level) is modest or negligible.  
253 Since both bending and axial force (due to overturning effects) contribute to the longitudinal stress, each flange  
254 within each splice is subjected to a different stress history. Recognizing this, the time history of the longitudinal  
255 stresses at the extreme fiber of the splices (in the smaller connected column) was monitored for each flange within

256 each splice, for each of the NTH runs. The Interaction Ratio ( $IR$ ; as defined in the Notations section) is a convenient  
 257 indicator of the stress in the flange, normalized by the yield strength of the flange material, such that  $IR = 1.0$   
 258 implies tension yielding at the extreme fiber of the cross section. Table 1 provides an overview of the results of the  
 259 NTH simulations for the three frames.

260 **Table 1 – Summary of results from Nonlinear Time History Simulations**

Frame	Ground motions scaled to 10/50 hazard				Ground motions scaled to 2/50 hazard			
	$IR_{peak}^{median\ a}$	$IR_{peak}^{max\ b}$	$\Delta_{peak}^{median\ a}$	$\Delta_{peak}^{max\ b}$	$IR_{peak}^{median}$	$IR_{peak}^{max}$	$\Delta_{peak}^{median}$	$\Delta_{peak}^{max}$
4-story	0.16	0.30 (3E <sup>c</sup> )	1.1%	2.9% (2 <sup>d</sup> )	0.30	0.54(3E <sup>c</sup> )	2.4%	6.1% (2 <sup>d</sup> )
9-story	0.11	0.30 (2E <sup>c</sup> )	0.8%	1.6% (3 <sup>d</sup> )	0.23	0.72(2I <sup>c</sup> )	2.0%	5.4% (4 <sup>d</sup> )
20-story	0.18	0.72 (5E <sup>c</sup> )	0.6%	1.5%(16 <sup>d</sup> )	0.22	0.95(5E <sup>c</sup> )	1.1%	2.5%(2 <sup>d</sup> )

261 <sup>a</sup>The median value (calculated from 20 ground motions), based on the peak tension Interaction Ratio  $IR$  or Interstory  
 262 Drift ratio  $\Delta$  observed in each ground motion.

263 <sup>b</sup> The maximum value (calculated from 20 ground motions), based on the peak tension Interaction Ratio  $IR$  or  
 264 Interstory Drift ratio  $\Delta$  observed in each ground motion.

265 <sup>c</sup>Value in parentheses indicates location of occurrence of  $IR_{peak}^{max}$ , e.g. “3E” indicates 3<sup>rd</sup> story Exterior column while  
 266 “2I” indicated the 2<sup>nd</sup> story Interior column.

267 <sup>d</sup>Value in parentheses indicates location of occurrence of  $\Delta_{peak}^{max}$ , e.g. “4” indicates 4<sup>th</sup> story

268  
 269 The Table includes the maximum value and the median value of  $IR_{peak}$  determined from 20 NTH simulations (for  
 270 each of the scaling levels). The  $IR_{peak}$  value presented in the table reflects the combination of axial force and  
 271 moment that produces the peak tensile stress in any of the splice flanges. The corresponding flange is considered the  
 272 critical flange for that NTH run. Corresponding statistics are also presented for the peak interstory drift, i.e.  $\Delta_{peak}$   
 273 (observed in any of the stories within a NTH run). Referring to the Table, the following observations may be made  
 274 regarding frame and splice response –

- 275 1. For the four-story frame, the interaction ratios are fairly modest, i.e.  $IR_{peak}^{max}$  for the 10/50 and 2/50 motions are  
 276 0.30 and 0.54 respectively. This suggests that for low rise frames, the tensile stress in the flanges is well below  
 277 the yield stress. This is consistent with intuition because (1) the response of the 4-story frame is dominated by  
 278 the first mode resulting in points of inflection near the center of the columns; thereby lowering the moment at  
 279 the splice and (2) the effects of overturning moment, and the associated axial tension are modest as well.
- 280 2. For the 9-story frame, the  $IR_{peak}^{max}$  for the 0.30 and 0.72 for the 10/50 and 2/50 motions respectively. These are  
 281 somewhat larger as compared to the corresponding values for the 4-story frames, presumably because both the  
 282 effects described above, i.e. mode of deformation as well as overturning moments are more prominent.  
 283 However, even these are significantly lower as compared to the capacity of the smaller connected column.

284 3. The splices in the 20-story frame are subjected to demands that are by far the most severe. For this frame,  
285  $IR_{peak}^{max}$  for the 10/50 and 2/50 are 0.72 and 0.95 respectively, indicating that demands approach the capacity of  
286 the smaller connected column (for the 2/50 hazard), due to a combination of higher-mode response, overturning  
287 effects and the larger dynamic forces.

288

289 Referring to Table 1, for all the frames, the interstory drift ratios are in the anticipated range. While the peak tensile  
290 stress (implied by  $IR_{peak}$ ) is an important parameter with respect to splice fracture, it is not appropriate to entirely  
291 disregard history effects in the development of the loading protocol, since the material at the tip the of UWR is also  
292 subject to local inelastic cyclic strain. To address this, a rigorous approach was adopted following the methodology  
293 originally developed for moment frame connections by Gupta and Krawinkler (1999), subsequently adapted by  
294 Richards and Uang (2006) and more recently Fell *et al.* (2009) for other components. Figure 3 schematically  
295 illustrates the loading protocol developed during this study for application to splice specimens. A detailed  
296 description of protocol development is provided in Shaw (2013), whereas the main features are briefly summarized  
297 below –

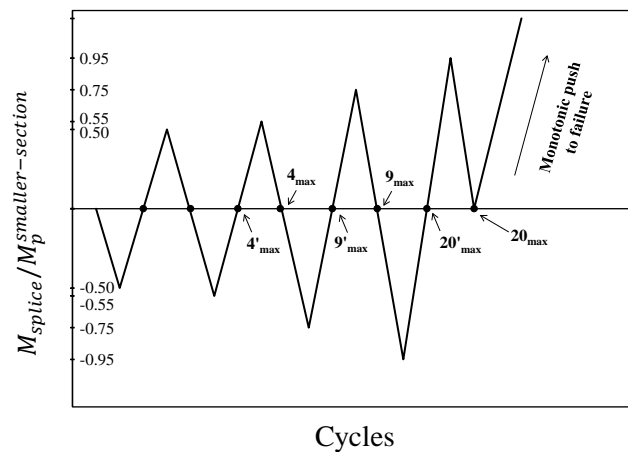
298 1. The primary objective of the loading protocol is to subject the PJP welds in the splice tests to stresses (including  
299 stress peaks and stress histories) that represent conservative as well as realistic demands consistent with specific  
300 seismic hazards.

301 2. The protocol is constructed in terms of the ratio  $M_{splice}/M_p^{smaller-section}$ , where  $M_{splice}$  is the applied (or  
302 “demand”) moment and  $M_p^{smaller-section}$  is the plastic moment capacity about the major axis of the smaller  
303 column section, including the effect of material overstrength, i.e.  $M_p^{smaller-section} = R_y F_y Z_x$ . Although the  
304 stresses in the splices (in archetype frames and in the NTH simulations) are a result of axial force and moments,  
305 the test apparatus (discussed in the next section) can apply only bending loads. The loading protocol was  
306 developed such that the longitudinal stresses in the flange generated in the bending-only configuration are  
307 consistent with those implied by the NTH simulations, which are a combination of axial and bending stresses.

308 3. Careful consideration was given to stress-history effects. For this purpose, the following steps were carried out:  
309 (1) each stress history was converted into equivalent constant amplitude cycles using the Rainflow Counting  
310 method (Matsuishi and Endo, 1968) (2) based on these equivalent cycles, a statistical analysis of the important  
311 history parameters (e.g. the peak interaction ratio, the number of damaging cycles, and cumulative stress

312 amplitudes) was conducted with respect to the response data from the different ground motions (3) at this point,  
 313 the protocol was heuristically constructed to match or exceed specific statistical indicators (percentile values) of  
 314 these history parameters. As discussed previously, Shaw (2013) provides a detailed description of these history  
 315 parameters, the rationale underlying their selection, and their use in the development of the protocol.

316 4. Referring to Figure 3, the loading protocol indicates several checkpoints marked by text on the loading history.  
 317 For example, one of the points is identified as “9<sub>max</sub>”. The implication is that at this instant in the protocol, all  
 318 the history indicators (indicative of damage) have been exceeded with a 100% probability in the critical flange  
 319 of the 9-story frame, for all ground motions scaled to the 2/50 hazard. Note that this is more conservative than  
 320 the benchmark established by Gupta and Krawinkler (1999) for qualification for welded-beam-to-column  
 321 connections (which utilized 86 percentile values from the 10/50 motions). The implication of this is that if a test  
 322 specimen survives a particular checkpoint on the protocol, it suggests that the connection is a candidate for  
 323 qualification under demands implied by that checkpoint. By extension, survival through the entire protocol  
 324 suggests that the splice detail may withstand demands consistent with those in 4-, 9- and 20- story buildings.



332 **Figure 3 – Loading Protocol**

333

334 The next section describes the full-scale testing on column splices based on this protocol, along with a summary of  
 335 ancillary material testing.

336  
 337  
 338  
 339

**SPLICE COMPONENT TESTS – SPECIMEN FABRICATION, ANCILLARY TESTING AND EXPERIMENTAL RESPONSE**

340  
341  
342

343 This section provides a detailed overview of the splice component tests, including the test setup, instrumentation,  
344 specimen fabrication, and finally, the test results. Table 2 includes the test matrix summarizing key features of the  
345 five tests that were conducted. Also included in Table 2 are some of the test results, discussed later. Referring to the  
346 Table, the column sizes used in these experiments are consistent with those commonly used in design practice. For  
347 example, Specimen #14A features one of the heaviest available W-sections (W14×730 connected to a W14×550).  
348 The tests may therefore be considered “full-scale.”

349 **Table 2 – Test Matrix and summary of key results**

Test	Specimen details			Results <sup>4</sup>			
	Column Sizes	Weld Pen	Remarks <sup>3</sup>	$\frac{M_{splice}^{max}}{M_p^{smaller-section}}$	$\frac{V_{splice}^{max}}{V_y^{smaller-section}}$	$\frac{\sigma_{flange}^{max}}{F_y^{flange}}$	$\frac{\delta_{midspan}}{\delta_y}$
24A	W24×370 W24×279	82% F <sup>1</sup> 87% W	Single external bevel, no access hole	1.13	0.85	1.31	4.8
24B	W24×370 W24×279	82% F 87% W	Single external bevel, no access hole	1.19	0.89	1.33	5.8
14A	W14×730 W14×550	82% F 87% W	Double beveled with access hole	1.37	0.93	1.34	16.1
14B	W14×455 W14×342	55%+ 40% <sup>2</sup> F 84% W	Double beveled with no access hole, internal flange weld terminated short of web fillet	1.24	0.86	1.34	5.0
14C	W14×145 W14×132	89% F 0% W	Single external bevel, no access hole, bolted web plate	1.04	0.72	1.43	2.0

350 <sup>1</sup>Flange and web welds denoted F and W respectively.  
351 <sup>2</sup>55% External flange weld, with 40% Internal flange weld terminated short of web fillet (see Figure 5c).  
352 <sup>3</sup>All details are shown schematically in Figure 5.  
353 <sup>4</sup>All referenced material properties are measured (see Table 3), rather than specified.  
354  
355

356 **Specimen Construction Process**

357 Since the performance of the PJP splices is sensitive to the execution of the weld details, it is especially important  
358 that the welds in the test specimens are representative of field welds. To ensure this, specimen fabrication and  
359 erection, including weld procedures, closely followed the processes and practices consistent with field  
360 implementation. The following process was implemented –

- 361 1. Steel column sections were procured from an AISC certified fabricator and erector. Mill certificates  
362 summarizing material yield, ultimate, and toughness properties were provided along with these sections. Data  
363 from these mill certificates is provided in Table 3.

- 364 2. The sections were shipped to a fabricator where the connection details were prepared; this included surface  
365 preparation for the weld bevels and the fabrication of erection plates.
- 366 3. The site-ready sub-assemblies were shipped to a steel erector where column sections were welded in a vertical  
367 position in an effort to minimize variance from field conditions.
- 368 4. These types of groove welds are not currently allowed in seismic force resisting systems. As a result, a new  
369 Welding Procedure Specification (WPS) was created for these welds. While details of the WPS are available in  
370 Shaw (2013), the main parameters of the WPS were as follows –
- 371 • FCAW-S welding with E70T-6 electrode (Lincoln NR-305); 3/32 inch diameter.
  - 372 • Deposit rate (travel speed) = 12-10 inches/minute.
  - 373 • Minimum preheat temperature 350°F (note that this is conservatively in excess of the 225°F minimum  
374 required by AWS D1.1, 2004, owing to the jumbo sections being welded); interpass temperature  
375 between 350 – 500°F.
  - 376 • Current 430-470 Amps, Voltage 25-26V.
- 377 5. A Procedure Qualification Record (PQR) was created to support the Welding Procedure. Data from the PQR  
378 testing (on a mockup assembly constructed to represent the splice welds) is provided in Table 3, along with  
379 similar data for the base metals (obtained from the mill certificates).
- 380 6. Upon completion, all the welds were inspected visually and with ultrasonic testing by independent inspectors.  
381 During this process, a crack was discovered at the root pass of Specimen #14C. The deficient weld was  
382 removed and re-welded. Subsequent inspection of the repaired weld revealed no cracks.

383

384 The above aspects are common to all specimens; specific weld details are discussed in the subsection on  
385 experimental response.

386

387

388

389

390

391

392 **Ancillary Testing for characterization of material toughness and constitutive properties**

393 The large scale tests were complemented by a comprehensive program of ancillary tests, summarized in Table 3.

394 Table 3 also summarizes the permissible values for each quantity measured in the ancillary tests.

395 **Table 3 – Material tensile and toughness data from ancillary testing**

Material source ↓		$F_y^2$ (ksi)	$F_u^2$ (ksi)	$F_y/F_u^2$	Elongation <sup>2</sup> (%)	CVN <sup>2</sup> at 0°F ft-lb	CVN <sup>2</sup> at 70°F ft-lb	CVN <sup>2</sup> at 70°F ft-lb
Applicable requirement <sup>1</sup> →		50-65 ksi	≥65 ksi	≤0.85	≥21%	≥ 20 ft-lb		≥20 ft-lb
Base metal Test 24A	W24X370	55.1	70.3	0.78	34	Not applicable		149
	W24X279	56.8	71.7	0.79	39			200
Base metal Test 24B	W24X370	54.5	70.2	0.78	38			149
	W24X279	56.9	71.9	0.79	33			200
Base metal Test 14A	W14X730	56.2	71.0	0.79	34			292
	W14X550	53.8	70.5	0.76	38			227
Base metal Test 14B	W14X455	57.0	73.9	0.77	36			297
	W14X342	52.8	71.3	0.74	28			104
Base metal Test 14C	W14X145	75.4 <sup>4</sup>	87.2	0.86 <sup>3</sup>	21			Not applicable <sup>4</sup>
	W14X132	54.2	77.7	0.70	31			
Weld	PQR	All-weld coupons were not tested for tensile properties, only toughness tests were conducted				52	Not tested	Not
	W14B post test					Not tested	50	Applicable

396 <sup>1</sup>Based on AISC 341-10 (2010).

397 <sup>2</sup>Average data from 3 coupon tests.

398 <sup>3</sup>Does not meet applicable standard.

399 <sup>4</sup>Base material toughness requirements are only applicable to heavy sections, both W14×145 and W14×132 are not  
400 categorized as “heavy” as per *The Steel Construction Manual* (AISC 360-11, 2011).

401

402 Referring to the Table, the program comprised the following types of tests:

403 1. Tension tests: A total of 30 coupons (3 replicates from the smaller column and larger column section of each of  
404 the five large scale test specimens). The main purpose of these tests was to establish yield and ultimate  
405 properties for the base materials. Referring to Table 3, the yield, ultimate and elongation properties are mostly  
406 within the permissible range, with the exception of the material for W14×145, for which the strengths are higher  
407 than the maximum allowable. However, note that W14×145 is the larger column within Specimen 14C, whereas  
408 the test protocol and benchmark performance is expressed in terms of the strength of the smaller column.

409 2. Charpy V Notch tests: Tests were conducted on coupons extracted from the base as well as weld material. For  
410 the base material (heavy sections), AISC 341-10 (2010) requires a minimum CVN toughness of 20 ft-lb at 70°F  
411 for specimens extracted from the core of the cross section. For demand-critical welds, the minimum  
412 requirement is 20 ft-lb at 0°F. In addition, a value of 40 ft-lb at 70°F from heat input envelope testing is also  
413 required for the weld filler metal (i.e. to qualify the electrode). To support the weld procedure specifications for



414 the current testing program, and to provide insight into the response of the fabricated connections, the following  
415 supplementary data was obtained –

- 416 a. CVN coupons from the PQR (Procedure Qualification Record) weld assembly: This involved the  
417 testing of CVN coupons at 0°F, to demonstrate that the joint could meet the specific standard (i.e.  
418 AISC 341-10), i.e. exhibit a CVN energy of 20 ft-lb at this temperature. Referring to Table 3, a value  
419 of 52 ft-lb (well in excess of 20 ft-lb) was obtained.
- 420 b. CVN coupons from the compression flange of Test Specimen 14B: Additional CVN coupons were  
421 extracted from the compression (un-fractured) flange of one of the full-scale test specimens after the  
422 completion of the test; these were tested at 70°F. The toughness data from these tests does not reflect  
423 the intent of the standard (AISC 341-10, 2010) given that the compression flange is subjected to  
424 several inelastic cycles before the CVN extraction and testing. However, these tests provide an  
425 indication of the toughness of the as-deposited weld at room (or test) temperature. The average CVN  
426 value (from 3 coupons) was 50 ft-lb.

427 In addition to establishing compliance with applicable standards, the ancillary tests serve the following purposes (1)  
428 they enable the interpretation of full-scale data with respect to measured, rather than specified material properties,  
429 and (2) they enable the calibration of material constitutive and fracture toughness properties in Finite Element  
430 simulations (discussed in a subsequent section).

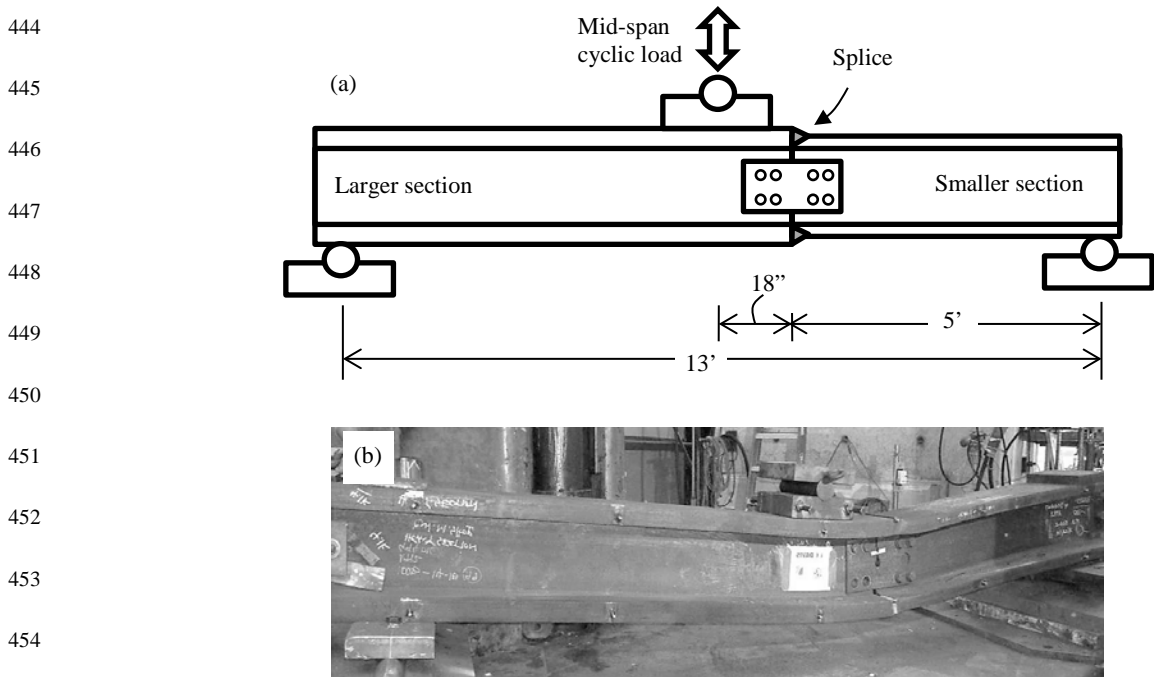
431

### 432 **Test Setup and Instrumentation**

433 Figure 4 schematically illustrates the test setup used for testing. Several factors controlled the design of the setup;  
434 these included limitations in the size, configuration and capacity of the testing machine as well as the necessity to  
435 provide loading and boundary conditions that reflected field conditions with realism. The main features of the test  
436 setup are now summarized with a discussion of some of the factors that controlled these features –

- 437 1. The specimens were all tested as beams in three-point bending, with a load applied at midspan. The splice is  
438 located at a distance of 18 inches from midspan, such that it is subjected to a combination of flexure and shear.
- 439 2. The testing machine applies load only in one (i.e. the downward direction). Cyclic loading was applied by  
440 rotating (i.e. flipping) the specimen about its longitudinal axis after every loading excursion implied by the  
441 loading protocol shown previously in Figure 3. The loading apparatus cannot apply axial tension. However, as

442 discussed previously, the loading protocol is developed such that flange stresses are consistent with those  
443 produced due to a combination of axial tension and bending in building columns.



451

452

453

454

455

456 **Figure 4** – (a) Schematic illustration of test setup and (b) Specimen 14B overview after test

457 All specimens were loaded in an identical manner, i.e. cyclic loading was applied at midspan as per the loading  
458 protocol, until either failure was observed or the machine capacity was exceeded (this happened only in the case of  
459 Specimen #14A). Note that the values in the loading protocol are the moments at the splice location normalized by  
460 the expected strength (i.e.  $M_p^{smaller-section} = R_y F_y Z_x$ ) of the specimen; these were converted to an equivalent  
461 midspan load for testing. The specimens were extensively instrumented. The primary control variable was the  
462 midspan force, and the associated splice moment. The midspan and splice deflections were also monitored. Strain  
463 gages were placed at multiple locations, including the flanges of the splices and the webs. The purpose of the web  
464 strain gages (rosettes) was to examine the distribution of shear between the web and the flanges. These are  
465 especially relevant for the bolted web connection (Specimen #14C), in which the load path for the shear force is not  
466 as rigid as for the other (welded web) specimens. Secondary instrumentation was installed to monitor unanticipated  
467 response such as out of plane buckling. However, this type of response was not observed for any of the tests. The  
468 instrumentation was complemented by still and video cameras. Being supported by the Network for Earthquake

469 Engineering Simulation (NEES), all the data from the project is freely available for download from the NEES data  
470 repository.

471

## 472 **Test Matrix**

473 Referring to the test matrix shown previously in Table 2, five specimens were tested. The main consideration in the  
474 selection of the section sizes was realism, such that these sections are of a comparable scale to those typically  
475 specified in moment frames. Testing archetype-scale components is especially important in the context of weld  
476 fracture because (1) scale-effects in fracture (Bažant, 1984; Anderson, 1995) are well known, wherein fracture  
477 mechanics must be invoked, often with some subjectivity, to generalize test results (2) the thermo-mechanical  
478 process of heat-transfer, cooling and phase change that occur during welding affect weld toughness, and may be  
479 scale dependent, especially if multi-pass welds are used, and finally (3) the residual stress patterns in large  
480 specimens are likely to be different than those developed in small scale specimens due to the constraint to shrinkage  
481 provided by the larger sections. All details were designed in consultation with the steel fabricator, erector as well as  
482 AISC, to provide an efficient means of obtaining the desired level of weld penetration representative of future  
483 practice (if, based on this study, PJP welds are determined to be suitable for column splices). Following this (and  
484 referring to Table 2), the highlights of the test matrix are as follows –

485 1. *Tests #24A, 24B:* Two replicate specimens featuring W24 columns (specifically W24×279 attached to  
486 W24×370) were tested. The size of these sections is representative of usage in 15-20 story moment frame  
487 buildings. Figure 5a schematically illustrates the splice detail for these specimens. Referring to the Figure, the  
488 flanges (2.09 inches for the W24×279 and 2.72 inches for the W24×370) were connected with one PJP weld on  
489 the outside of the flange – equivalent to 82% penetration with respect to the smaller (W24×279) flange. Since  
490 only an external weld with a single bevel was used, a weld access hole was not provided in the web. The web  
491 featured a single beveled PJP weld with 87% with respect to the thinner (W24×279) web. A bolted erection  
492 plate, sized for erection loads was provided as also indicated in Figure 5a.

493 2. *Test #14A:* This specimen was fabricated from a W14×730 column connected to a W14×550; which are two of  
494 the heaviest available W-sections. In fact, the flange sizes are 4.91 and 3.82 inches for the larger and smaller  
495 columns respectively, requiring the largest possible weld in a column splice for W-sections. Figure 5b  
496 schematically illustrates the splice detail for this specimen. Referring to the Figure, the flanges were double

497 beveled, i.e. welds were provided on the inside and outside of the flanges. The total connected penetration was  
498 82% with respect to the smaller (W14×550) flange. A weld access hole (in compliance with AWS D1.8, 2009)  
499 was provided in the web. The web featured a single sided PJP weld with 87% penetration. Similar to the W24  
500 specimens, a bolted erection plate was provided. This plate was ground to follow the contour of the weld access  
501 hole.

502 3. *Test #14B*: This specimen was fabricated from A W14×455 column connected to A W14×342; which have  
503 flange sizes 3.21 and 2.47 inches for the larger and smaller columns respectively. Referring to Figure 5c, the  
504 flange of the smaller column was double beveled, similar to Specimen 14A. The external weld penetration was  
505 55%, whereas the internal weld penetration was 40% (with respect to the thinner flange). However, the internal  
506 bevel (and weld) was stopped short of the web fillet. Thus, the detail was designed to examine the performance  
507 of a cost-effective connection that did not require a weld-access hole. From a fracture mechanics perspective,  
508 this absence of the continuous weld on the inside of the flange generates a large unfused area in the k-region of  
509 the columns. An erection plate was provided, similar to the W24 specimens.

510 4. *Test #14C*: This specimen features the smallest specimens, i.e. a W14×145 connected to a W14×132. These  
511 member sizes are representative of those typically used in low-mid rise frames (i.e. 2-5 stories tall), which  
512 constitute a large percentage of the building stock. The flange of the smaller column was provided with a single,  
513 external bevel and a PJP weld with 89% penetration. No weld access hole was provided. The distinguishing  
514 characteristic of this specimen was that the webs of the columns were not welded; rather a bolted web-splice  
515 plate was provided for shear transfer between the webs. Post-Northridge research (FEMA, 2000) indicated that  
516 bolted webs are inefficient in transferring shear, producing secondary bending in the flanges, increasing the  
517 susceptibility to premature fracture. However, referring to previous discussion, Table 1, and the loading  
518 protocol shown in Figure 3, recall that the force demands for low-mid rise frames are rather modest, with  
519  $IR_{peak}^{max} < 0.5$ . With this consideration, Specimen 14C was designed in this manner to explore the possibility of  
520 an economical connection for low-mid rise frames. The web plate was designed to develop the full shear  
521 capacity of the web, and the bolt pattern was determined assuming an eccentrically loaded bolted connection  
522 (Shaw, 2013). Figure 5d illustrates this detail schematically.

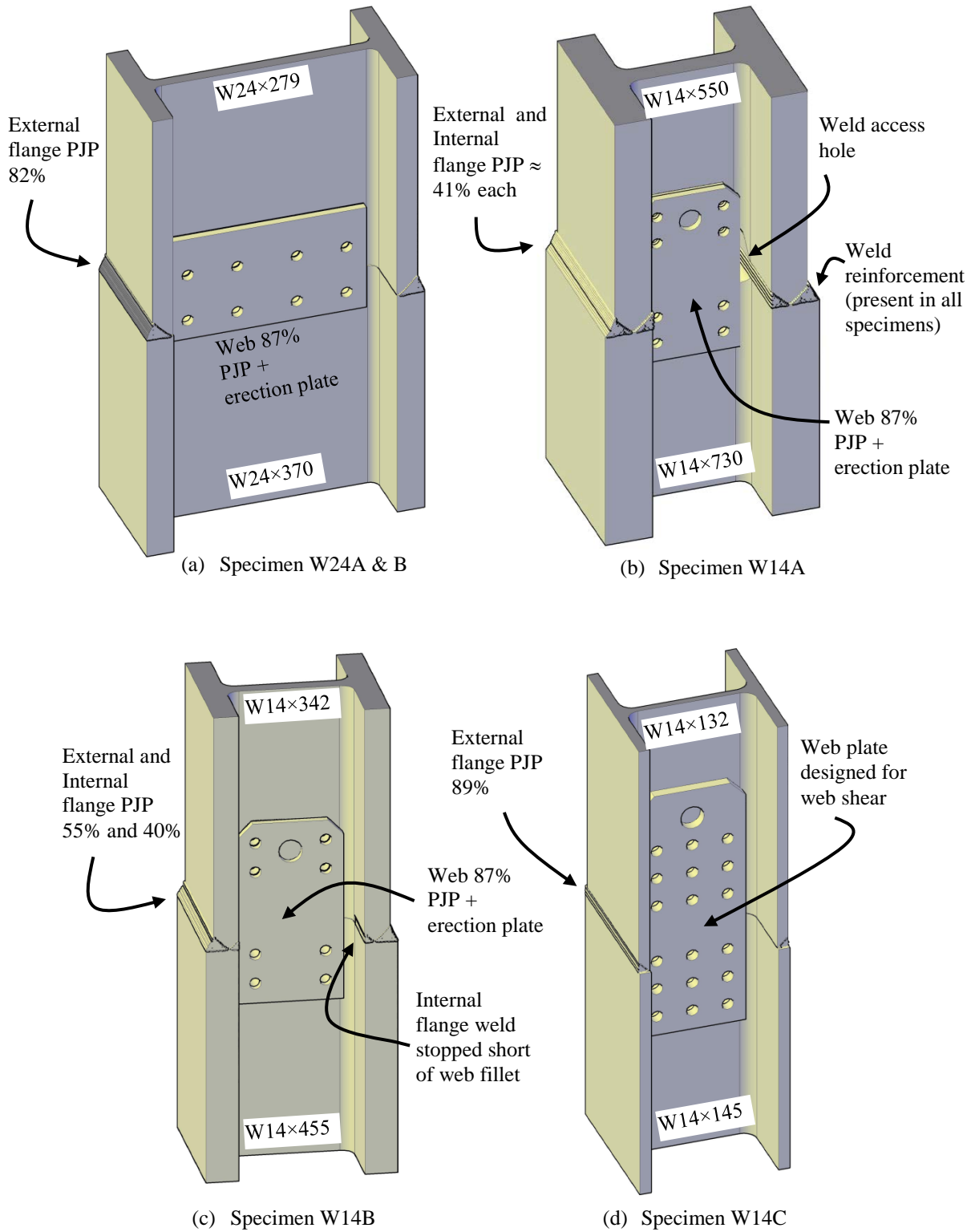


Figure 5 – Splice connection details

524 For all the specimens, a smooth transition was obtained between the thicker and the thinner flange (indicated on  
525 Figure 5a, but representative of all the specimens), in compliance with AWS D1.8 (2009). This has two implications  
526 (1) the flared shape of the weld provides reinforcement at the section of the UWR (2) no sharp discontinuities or re-  
527 entrant corners, other than the UWR itself, are present in the detail. The next section describes the qualitative and  
528 quantitative results from the splice experiments.

529

### 530 **Experimental observations**

531 Table 2 introduced previously summarizes results from all the tests. All the specimens survived the cyclic portion of  
532 the loading history (shown in Figure 3), and all (with the exception of Specimen #14A, which did not fail since  
533 machine capacity was reached) failed during the final monotonic push. This implies that all specimens exhibited  
534 excellent performance when assessed in the context of demands imposed by the loading protocol. Figures 6 a-d  
535 illustrate the load-deformation response of all the splice connections. The loads indicated on Figure 6 are expressed  
536 in terms of the moment at the splice (normalized by the plastic moment, based on measured material properties)  
537 versus the midspan deflection. The primary indicators of performance are (1) the peak moment at the splice; this was  
538 always observed during the final cycle (2) estimated stress in the flange at the splice (3) peak shear at the splice.  
539 These quantities are summarized in Table 2. Other indicators of performance, such as the total deformation of the  
540 column provide a general, qualitative understanding of specimen response. The following discussion, which outlines  
541 the test data from each of these splices individually, is based on these results presented in Table 2 and Figure 6.

542

543

544

545

546

547

548

549

550

551

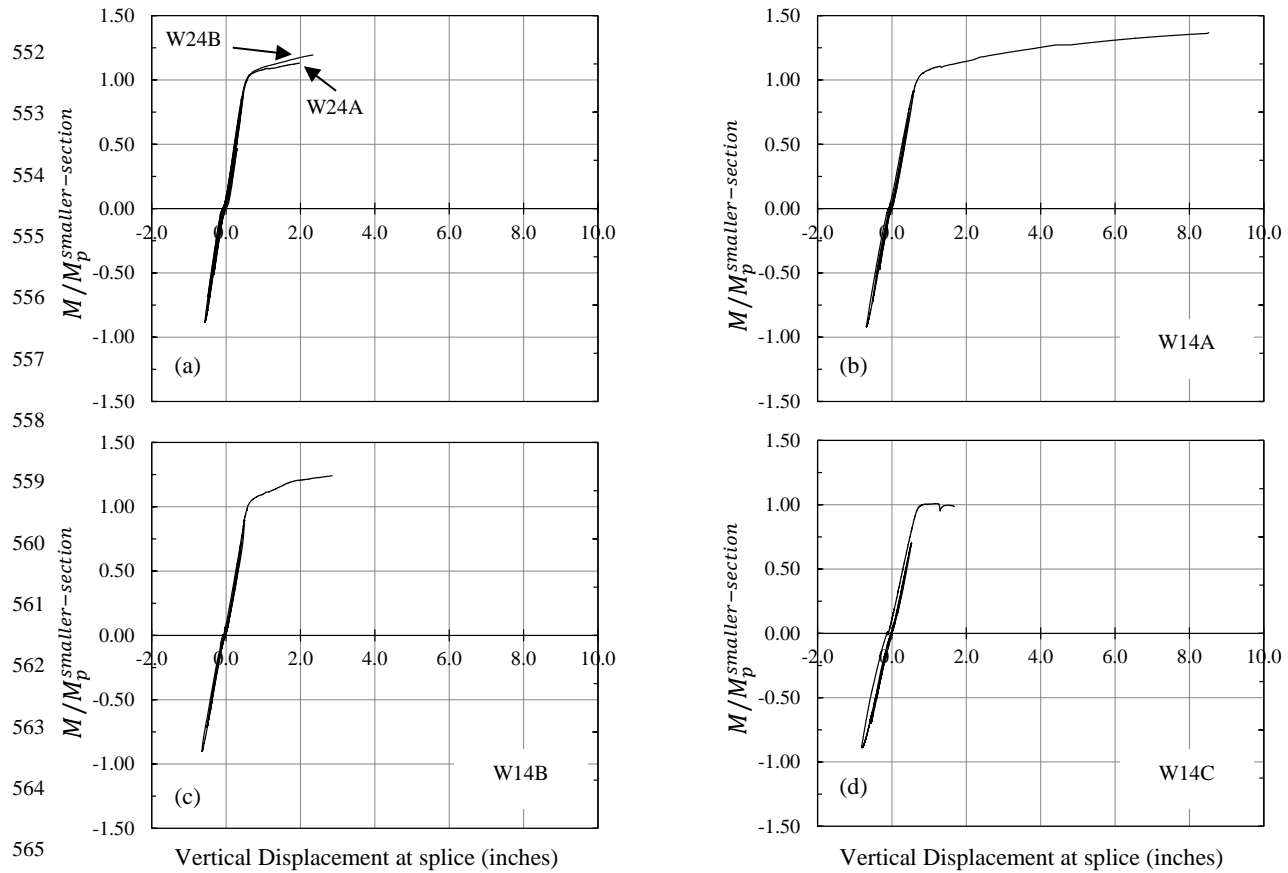


**Figure 6** – Load displacement curves for full-scale tests (a) W24A&B (b) W14A (c) W14B (d) W14C

Response of Specimens 24A and 24B: Referring to Figure 6a, both these specimens exhibited virtually identical response. The initial cycles produced no observable signs of distress. However, during the cycles with amplitude  $0.95M_p$ , minor flaking of the mill scale was observed in the vicinity of the splice, indicating the onset of yielding. During the final, monotonic push, widespread yielding was observed in the splice region, as well as the surrounding areas, including in both the smaller and the larger column sections. The test was concluded when fracture was suddenly observed at a force corresponding to the development of the splice moment  $M_{splice} = 1.13 \times M_p^{smaller-section}$  for Specimen 24A and  $M_{splice} = 1.19 \times M_p^{smaller-section}$  for Specimen 24B. The fracture initiated at the tip of the UWR and the surface was coincident with the Heat Affected Zone (HAZ). Based on an inverse section analysis (using the measured stress-strain data from the materials), weld stress at the instant of fracture was estimated to be  $\sigma_{flange} \approx 1.32 \times F_y^{flange}$  (where  $F_y^{flange}$  is the measured yield stress of the particular section – See Table 3). This suggests that the weld was fully yielded at the PJP section, and that the net section strength of this section was achieved. Also at this instant, the shear force in the splice was  $V_{splice} = 0.85 \times V_y^{smaller-section}$ , where

580  $V_y^{smaller-section} = 0.6 \times F_y \times A_{web}^{smaller-section}$ . The fracture completely severed the tension flange and propagated  
581 up through the PJP weld in the web, severing most of the web. Several bolts in the erection plate fractured as the  
582 crack propagated through the web weld. Figures 7a and b show photographs of both the tests taken after fracture.

583

584 *Response of Specimen 14A:* Similar to the Specimen 24A and 24B, the initial loading cycles produced no observable  
585 signs of distress in the specimen. However, during the cycles with amplitude  $0.95M_p$ , minor flaking of the mill scale  
586 was observed in the vicinity of the splice, indicating the onset of yielding. During the final push, large scale yielding  
587 was observed in the splice, accompanied by widespread flaking of mill scale and the formation of visible slip bands.  
588 Figure 6b shows the load-deformation response, whereas Figure 7c shows a photograph of the specimen after the  
589 conclusion of the experiment. Referring to the Figure, fracture propagation was not observed for this experiment,  
590 which had to be concluded owing to safety concerns, wherein the applied load approached the capacity of the  
591 laboratory strong floor. Shown in Figure 7d is a close up view of the unfused weld root. Small cracks  
592 (approximately 0.5 inches long) initiated at both tips. The degree of inelastic deformation in this specimen is  
593 striking. At the conclusion of the test, the estimated weld stresses are  $\sigma_{flange} \approx 1.34 \times F_y^{flange}$ . At this time, the  
594 moment in the splice was  $M_{splice} = 1.37 \times M_p^{smaller-section}$ , whereas the shear in the splice was  $V_{splice} = 0.93 \times$   
595  $V_y^{smaller-section}$ .

596

597 *Response of Specimen 14B:* Similar to the other specimens, the initial loading cycles produced no observable signs  
598 of distress in the specimen. During the final push, large scale yielding was observed in the splice, accompanied by  
599 widespread flaking of mill scale and the formation of visible slip bands. Figure 6c shows the load-deformation  
600 curve, while Figure 7e shows a photograph of the specimen after the conclusion of the experiment. Qualitatively, the  
601 response of the specimen was similar to that of Specimen 14A, except that fracture was observed during the final  
602 push, when the moment in the splice was  $M_{splice} = 1.24 \times M_p^{smaller-section}$ , whereas shear in the splice was  
603  $V_{splice} = 0.86 \times V_y^{smaller-section}$ . The estimated weld stresses (based on strain gage data) are  $\sigma_{flange} \approx 1.34 \times$   
604  $F_y^{flange}$ .

605



606 *Response of Specimen 14C:* Specimen 14C featured a bolted web plate, with no weld connection between the webs.  
607 Figures 6d and 7f show the load-deformation curve and post-test photograph respectively. The response of this  
608 specimen was somewhat different than the other specimens, primarily in that yielding was observed at lower  
609 moments; in fact, some yielding was observed even in the cycles corresponding to  $0.75M_p$ . This may be attributed  
610 to the absence of full stress transfer through the web, in the tension region such that development of full moment  
611 capacity is not theoretically possible. However, fracture was not observed until the final push – Figure 7f shows a  
612 post-test photograph. At the time of fracture, the moment in the splice was  $M_{splice} = 1.04 \times M_p^{smaller-section}$ ,  
613 whereas the shear in the splice was  $V_{splice} = 0.72 \times V_y^{smaller-section}$ . Thus, even when judged relative to the entire  
614 loading protocol, the connection exhibited excellent performance. It is important to recall here that this detail, with  
615 the bolted web splice (and associated section sizes) are targeted towards low-rise structures, where the demands are  
616 quite low – refer, for example Table 1. When evaluated in this context, the response of the specimen is even more  
617 impressive. The strain rosette attached to the web splice plate recorded negligible shear strain. When combined with  
618 the observation that negligible shear deformation was noted in the flanges, this suggests that the shear was  
619 predominantly transferred through friction in the bearing portion of the sections, which provides the most rigid load  
620 path for the shear. This bearing zone develops as a result of the flexure in the cross section. Two points may be  
621 made based on this observation (1) Adequate friction was likely generated even in the absence of net axial  
622 compression, which is typically present in low-rise buildings, wherein overturning moments are low (2) Unlike  
623 moment connections, in which the shear tab separates the web of the beam from the flange of the column, friction  
624 may be a reliable mechanism of shear transfer in column splices where the sections are in direct contact. In  
625 summary, it appears that other than the loss of some flexural capacity (due to the unavailability of the web in the  
626 tension region), the absence of a welded web splice does not compromise the effectiveness of the connection in any  
627 significant way.

628

629

630

631

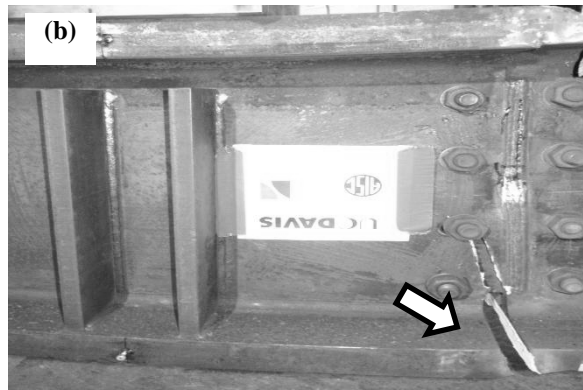
632

633

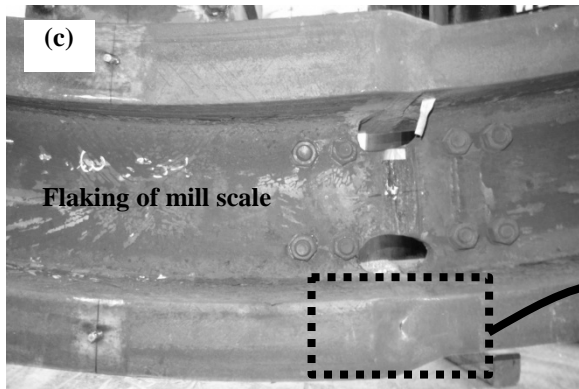
634  
635  
636  
637  
638  
639  
640  
641  
642  
643  
644  
645  
646  
647  
648  
649  
650  
651  
652  
653  
654  
655  
656  
657  
658  
659  
660  
661



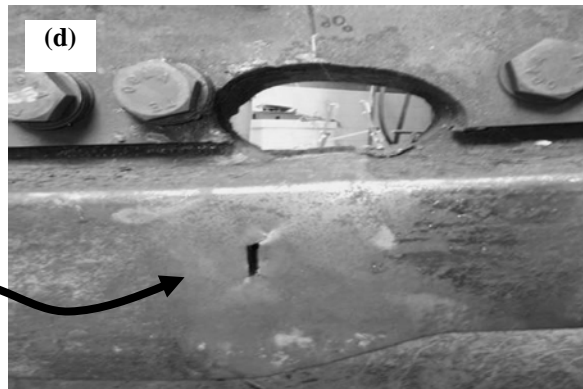
W24A



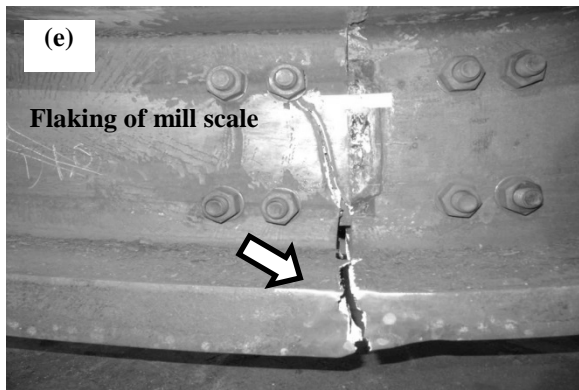
W24B



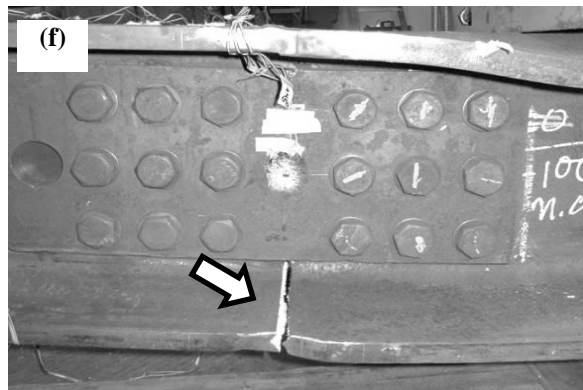
W14A Overview



W14A Close-up showing widening and growth of flaw



W14B



W14C

Figure 7 – Post-test photographs of all the specimens; block arrows indicate fracture

662 **Analysis and Discussion**

663 The preceding section provides specific discussion of individual specimen response. Based on this discussion,  
664 several general observations are now presented to evaluate the suitability of these types of connections in IMRF and  
665 SMRF structures in highly seismic regions. The main observations are –

- 666 1. All specimens survived the cyclic portion of the protocol, and all (with the exception of 14A) fractured on  
667 the final push. Recall that the protocol (if applied through completion) represents peak expected demands  
668 in 20 story buildings subjected to 2/50 ground motions. In this context, all the specimens (as tested in the  
669 lab) may be considered suitable candidates for application in such buildings.
- 670 2. In addition to exceeding the demands implied by the protocol, all the specimens also show significant  
671 inelastic deformation capacity. Referring to Table 2, the displacements (recorded at the midspan of the  
672 specimen) were several times yield displacement. Referring to previous discussion on demands, recall that  
673 column splices are mainly “force-controlled” components, with little expectation of inelastic action.
- 674 3. All the splice specimens were subjected to intense shear at the time of fracture. The shear demands in the  
675 these splices were in the range of  $0.72V_y^{smaller-section} - 0.93V_y^{smaller-section}$ . This is significantly higher  
676 than may be expected in archetype buildings, wherein high moments at the splice location (which is  
677 typically near the center of the column) are accompanied by low shear since this type of response is  
678 associated with single curvature bending of the column associated with higher mode response. Recall that  
679 the test setup utilized by Bruneau and Mahin (1991) did not apply shear to the splices.
- 680 4. Two of the specimens featured somewhat innovative details. These are (1) Specimen 14B which did not  
681 have a weld access hole, despite the presence of a weld on the inside of the web, and (2) Specimen 14C  
682 which did not feature a welded web splice. Both these details exhibited excellent performance.

683  
684 The above observations indicate that the as-tested details are suitable for resisting seismic demands in moment  
685 frames. However, additional analysis needs to be conducted to generalize the test results to evaluate the possibility  
686 of their implementation in field details. For example, while the observed performance exceeded anticipated  
687 demands, the material toughness properties (specifically the weld properties, see Table 3) also exceeded the  
688 minimum required. Thus, extrapolation of the test results to field details (for which only minimum toughness may be

689 relied upon, but which also will have reduced demands relative to the test splices) cannot be conducted without  
690 fracture mechanics analysis. The next section presents such an analysis.

691

692

### **FRACTURE MECHANICS ANALYSIS OF SPLICE CONNECTIONS**

693 The primary purpose of the fracture mechanics simulations presented in this section is to provide support for  
694 generalization of the experimental findings. The following points define the scope and intent of the simulations –

695 1. The main objective of the simulations is to examine the fracture toughness demands (represented by a stress  
696 intensity factor  $K_I$ ), and its relationship to applied stresses in the column flange. This relationship may be used  
697 to evaluate the suitability of current material toughness requirements for details similar to the ones tested in the  
698 study.

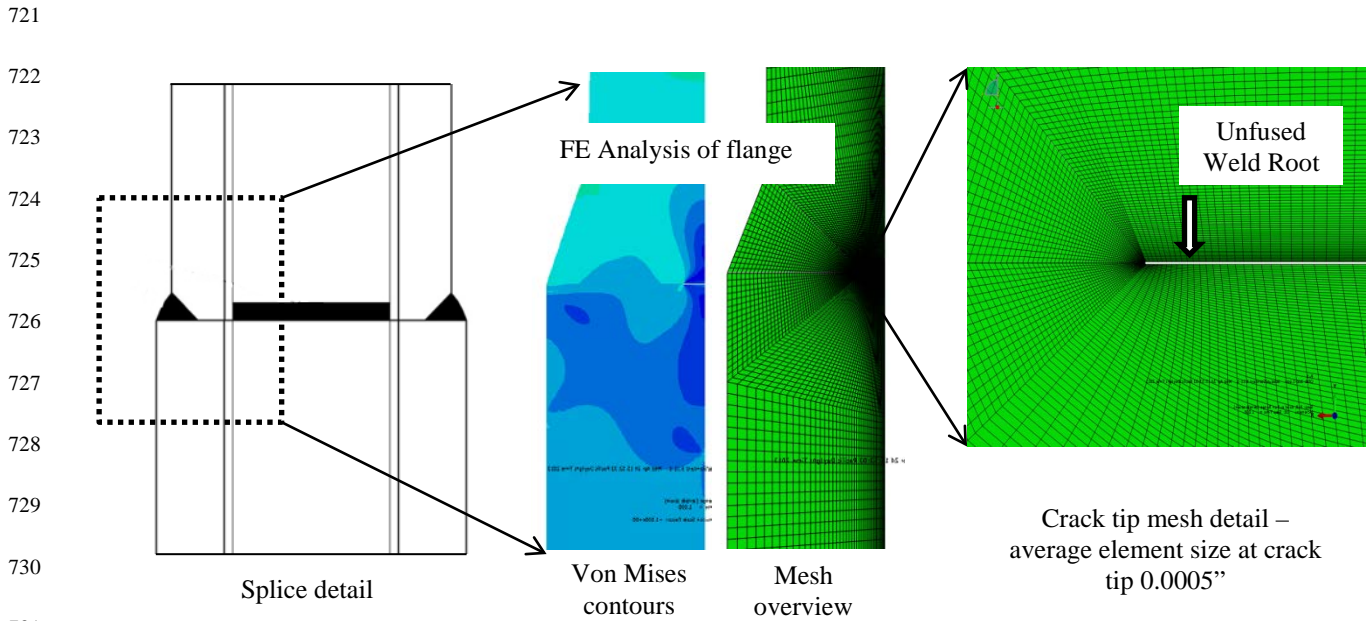
699 2. The simulations did not examine details distinct (in terms of shapes welded, extent of penetration or other  
700 features) from the ones tested in this study. This is because (1) in terms of configuration, it is anticipated that  
701 the test specimens represent key geometric aspects of PJP-welded splices, which may be considered for use in  
702 the future (2) the test splices are fairly large, and fracture mechanics results based on larger specimens are in  
703 general conservative when applied to geometrically similar details that are smaller (Anderson, 1995; Bazant,  
704 1984). Thus while not precise, a simulation of the test specimens provides a reasonable basis for extrapolation  
705 to similar details that are physically smaller in size, and (3) A full parametric study examining all possible types  
706 of splice details and sizes is prohibitively expensive.

707

708 Fracture mechanics simulations were conducted for the flange regions of four specimens, i.e. W14A, W24A & B  
709 (identical simulation, given that the specimens are nominally identical), and W14C. The specimen W14B was not  
710 simulated, since the termination of the internal weld would require 3-dimensional simulation. All simulations were  
711 conducted using the commercial platform ABAQUS (ABAQUS, 2012). Figure 8 schematically illustrates a Finite  
712 Element (FE) mesh for one such simulation (shown for the W24 specimen); the FE mesh for the W24 specimen is  
713 qualitatively similar. The mesh for W14A is somewhat different to accommodate the embedded crack with two  
714 crack tips (refer Shaw, 2013). Referring to the figure, the following points describe key features of the simulations –

715

716 1. All the simulations modeled only the flange region of the splices, subjected to pure tension. This is based on the  
 717 assumption that this loading state controls the fracture toughness demands at the UWR. As shown in Figure 8,  
 718 the models were 2-D plane-strain models, since stress variations through the width of the flange are relatively  
 719 modest and the plane strain approximation represents out of plane constraint in a conservative manner. This  
 720 modeling approach has been previously adopted with good agreement with test data by Nuttayasakul (2000).



732 **Figure 8** – Finite element simulation of splice flanges (W24 simulation shown as representative)

733 2. Each simulation featured approximately 20,000 plane strain 8-node quadrilateral elements (114,000 were used  
 734 for the W14A simulation, owing to the two crack tips). As indicated in the inset in Figure 8, the crack tip was  
 735 greatly refined at the tip of the flaw, such that the smallest element size was on the order of 0.0005 inches. The  
 736 crack tip was modeled with a diameter of 0.001 inches (significantly lower than the anticipated Critical Crack  
 737 Tip Opening Displacement  $CTOD_C$  for structural steels, which is typically on the order of 0.01 inches). This  
 738 type of FE mesh at the crack tip has been shown to adequately capture the stress gradients as well as the effects  
 739 of crack tip blunting through the work of McMeeking and Parks (1978), and then subsequently Kanvinde and  
 740 Deierlein (2006).

741 3. Material constitutive properties were based on von-Mises plasticity with isotropic hardening. For the base  
 742 material, the properties were calibrated from the coupon tests described previously and summarized in Table 3.

743 For the weld material, all-weld coupon data (for a similar type of weld) generated previously by Kanvinde *et al.*  
744 (2008) was used for calibration.

745 4. Loading was applied in the form of a stress traction on the smaller (top) flange as shown in Figure 8. The  
746 contour J-integral (Rice, 1968) was evaluated at each loading step. The J-integral is a well-established index for  
747 characterizing fracture toughness demands (and capacities) in steel component with small to moderate yielding.  
748 The ABAQUS platform provides functionality for calculation of the J-integral. For each loading step, the J-  
749 integral was calculated from approximately 40 contours around the crack tip to minimize numerical  
750 inconsistencies. The J-integral ( $J_I$ , where the subscript “I” denotes Mode I, or crack opening) may be converted  
751 an equivalent stress intensity factor  $K_I$  as per the following relationship, wherein  $E$  and  $\nu$  are the elastic  
752 modulus and Poisson’s ratio –

753

$$754 K_I = \sqrt{EJ_I / (1 - \nu^2)} \quad (1)$$

755

756 Figures 9a, b and c illustrate the results of the simulations for the W24, W14A, and W14C simulations respectively.  
757 To interpret these figures effectively, it is useful to consider relationships between the CVN energy (for which  
758 minimum values are required as per the Seismic Provisions) and the critical stress intensity factor  $K_{IC}$  (which is a  
759 measure of the fracture toughness capacity). One such relationship (based on statistical correlation) is provided by  
760 Barsom and Rolfe (1999). Equation (2) below illustrates this relationship –

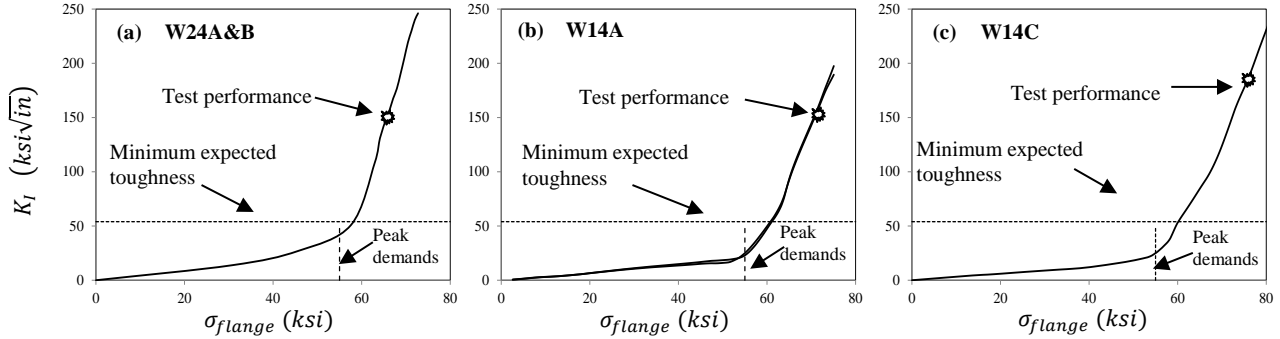
761

$$762 K_{IC}^{dynamic} = 0.001 \times \sqrt{5000 \times CVN \times E} \quad (2)$$

763

764 In the above equation  $CVN$  is the Charpy energy in ft-lb,  $E$  is the modulus of elasticity in ksi, and  $K_{IC}^{dynamic}$  is the  
765 stress intensity factor (in  $ksi\sqrt{in}$ ) under dynamic loading rates (since it is derived from the CVN data which is  
766 obtained from high-rate dynamic tests). In contrast, loading rates in the tests described in this paper, or even in field  
767 details subjected to earthquakes, may be considered “static,” since they are several orders of magnitude lower than  
768 those observed in CVN tests (Barsom and Rolfe, 1999). In general, the  $K_{IC}^{dynamic}$  is a lower bound on the available  
769 fracture toughness in seismic details. In each of the figures, the stress intensity factor  $K_I$  determined from the FE

770 simulations is plotted against the applied stress in the smaller flange. Since W14A has two crack tips, Figure 9b has  
 771 two curves. However, these are almost coincident indicating that the fracture toughness demand at both crack tips is  
 772 virtually identical.



779 **Figure 9** – Results of Finite Element Simulations for (a) W24 specimens (b) W14A, and (c) W14C

780 A close inspection of Figures 9a-c offers the following insights –

- 781 1. For all the simulations, the  $K_I$  increases, as expected, monotonically with respect to the applied stress level.  
 782 The points labeled “Test performance” on the figures indicate the estimated longitudinal stress in the flange  
 783 in each of the specimens at the time of fracture (based on an inverse sectional analysis outlined earlier).  
 784 Referring to these labels on the figure, these stresses are in 65-75 ksi range. At these stresses,  $K_I$  is in the  
 785 range of 150 – 200  $ksi\sqrt{in}$ , implying it to be the available fracture toughness at the crack tips in the full-  
 786 scale specimens. For comparison, if the CVN values from the PQR assembly (i.e. 52 ft-lb) or the post-test  
 787 weld from the W14B specimen (50 ft-lb) are converted to equivalent  $K_{IC}^{dynamic}$  values as per Equation (2),  
 788 then  $K_{IC}^{dynamic} \approx 85 \text{ ksi}\sqrt{in}$ . The difference (i.e. the significantly higher implied toughness in the splice  
 789 simulations as compared to  $K_{IC}^{dynamic} \approx 85 \text{ ksi}\sqrt{in}$  determined above) is not entirely surprising for the  
 790 following reasons (1) that both the PQR tests as well as the W14B CVN tests are dynamic, such that  
 791  $85 \text{ ksi}\sqrt{in}$  is a lower bound on the available toughness and (2) the PQR tests were conducted at a lower  
 792 temperature (i.e. 0°F), which is lower than the temperature at which the full-scale tests ( $\approx 60^\circ\text{F}$ ) were  
 793 conducted. In fact, the value  $K_I \approx 150 - 200 \text{ ksi}\sqrt{in}$  is in the range of fracture toughness values for  
 794 similar weld materials tested using static (rather than dynamic) fracture mechanics tests (Kanvinde *et al.*,  
 795 2008).

796 2. In each of the Figures 9a-c, the marker “Peak Demands” indicates the maximum anticipated stress in the  
797 splice flange based on the NTH simulations described earlier – this is equal to the expected yield stress, i.e.  
798 approximately 55 ksi. Based on the intersection of this marker with the curves in Figures 9a-c, the  
799 toughness demand at this value of flange stress is  $45 \text{ ksi}\sqrt{\text{in}}$ ,  $26 \text{ ksi}\sqrt{\text{in}}$ , and  $27 \text{ ksi}\sqrt{\text{in}}$ , for W24, W14A,  
800 and W14C respectively. Also shown in the figures is the horizontal line labeled “Minimum expected  
801 toughness.” This value  $K_{IC} = 54 \text{ ksi}\sqrt{\text{in}}$  is obtained by substituting  $\text{CVN} = 20 \text{ ft-lb}$  into Equation (2). The  
802 value of 20 ft-lb may be considered a suitable lower bound for material toughness based because (1) for the  
803 weld filler metal, a value of 20 ft-lb at 0°F is required, and (2) for heavy sections, i.e. base metal, a CVN  
804 value 20 ft-lb at 70°F in the core of the section is required; toughness elsewhere will likely be higher. As a  
805 result,  $K_{IC} = 54 \text{ ksi}\sqrt{\text{in}}$  is a reasonable lower bound on the expected toughness in a demand critical weld,  
806 such as the PJP welds in splices. Relative to this value, the demands are lower (see Figure 9), suggesting  
807 that the splice details tested in this study are suitable for field use even if a low estimate of material  
808 toughness is considered. A possible exception to this is in the case of buildings where the column splices  
809 may be exposed to low temperatures (i.e.  $\leq 50^\circ\text{F}$ ), since the base metal toughness requirement (20 ft-lb) is  
810 applicable at 70°F. The Seismic Provisions (AISC 341-10) require that “*the minimum qualification*  
811 *temperature for AWS D1.8/D1.8M Annex A be adjusted such that the test temperature for the Charpy V-*  
812 *notch toughness qualification tests be no more than 20 °F (11 °C) above the lowest anticipated service*  
813 *temperature (LAST).*”

814  
815 In summary, the FE simulations provide quantitative insight into the relationships between fracture toughness  
816 demands and applied stresses. For the connection details tested in this study, it is apparent that the toughness  
817 demands are lower as compared to the minimum available toughness capacity. This provides a suitable basis for  
818 generalizing the test results to connections that are geometrically similar to (and smaller than) the ones tested in this  
819 study. The next section summarizes the study along with its findings, implications, and limitations.

820  
821  
822  
823



## SUMMARY AND CONCLUSIONS

824  
825 Current design standards (AISC 341-10, 2010) require the use of Complete Joint Penetration (CJP) groove welds for  
826 column splices in Intermediate and Special Moment Frames in seismic design. These requirements are a result of  
827 research following the Northridge Earthquake on Welded Beam Column connections (SAC, 1996) that  
828 demonstrated the detrimental effect of embedded flaws (such as those produced at Partial Joint Penetration welds)  
829 on the response of welded joints. However, more recent research (Myers *et al.*, 2009; Gomez *et al.*, 2010; and  
830 Dubina and Stratan, 2002) indicate that when high-toughness materials are used (as also mandated by post-  
831 Northridge design standards), then excellent performance may be obtained even if a flaw is present. Motivated by  
832 this research, the main objective of the current study is to examine the feasibility of PJP-welded column splices for  
833 steel moment frame construction in seismic regions.

834  
835 The main scientific component of this study is a series of five full scale column splice tests. The full-scale tests are  
836 supported by a comprehensive program of Nonlinear Time History (NTH) simulation as well as ancillary material  
837 tests. The objective of the NTH simulations is to quantitatively establish force and moment demands in the splices,  
838 ultimately leading to the development of a loading protocol for the full-scale experiments. The ancillary tests enable  
839 the interpretation of full-scale test data with respect to measured, rather than specified material properties. The  
840 program of testing is also complemented by Finite Element simulations that employ fracture mechanics to develop  
841 support for the generalization of test results.

842  
843 The full-scale test matrix includes a range of column sizes and details. The key variables interrogated in the test  
844 matrix include (1) column size; such that the tested specimens included sections from W14×132 to W14×730 with  
845  $\approx 5$  inch thick flanges, as well as two specimens featuring W24 sections. The sizes represent commonly used  
846 sections for 4-20 story buildings (2) weld details; including single-bevel (W14C, W24A & B), and double-bevel  
847 specimens with (W14A) and without (W14B) a weld-access hole and (3) the absence of a welded web on one of the  
848 specimens (W14C) to examine the feasibility of bolted web connections for low-rise construction where the  
849 demands are modest.

850

851 The specimens were all subjected to reversed cyclic loading as per a loading protocol based on the NTH simulations.  
852 The load was applied in a three-point bend configuration such that the splice was subjected to a combination of  
853 flexure and shear. All the specimens exhibited excellent performance, surviving the entire loading protocol. Four out  
854 of the five specimens fractured in the tension flange of the splice during the final monotonic push after completion  
855 of the protocol. One specimen (W14A) did not fracture before machine capacity was reached, requiring the  
856 termination of the test. All specimens showed a high degree of inelastic deformation prior to fracture with yielding  
857 in both the larger and smaller column. Given that inelastic action is not expected in column splices (based on design  
858 intent as well as NTH simulation), this performance is especially impressive. The peak moment sustained by the  
859 splices was in the range of  $1.04 \times M_p^{smaller-section}$  (for the bolted web, i.e. W14C specimen) to  $1.37 \times$   
860  $M_p^{smaller-section}$  for the W14A specimen, indicating that these splices developed the strength of the smaller  
861 connected column. The shear in these splices ranged from  $0.72V_y^{smaller-section} - 0.93V_y^{smaller-section}$ ; these  
862 combinations of high moment and shear are highly unlikely in an archetype frame.

863

864 A series of fracture mechanics simulations was conducted to develop support for the generalization of test results.  
865 The main objective of the FE simulations was to examine the relationship between the fracture toughness demand  
866 (represented by the stress intensity factor  $K_I$ , and the applied stress in the flange). The simulations indicated that for  
867 the tested connections, the toughness demands are below the minimum expected toughness (considering the  
868 requirements of AISC 341-10, 2010). This suggests that details similar to the ones tested in the study may be  
869 suitable for general use in the field. While the results of the study are encouraging from the perspective of adoption  
870 of PJP splices in IMRFs and SMRFs, the study has several limitations that must be considered when interpreting the  
871 results. These are now summarized in a point-wise manner –

- 872 1. While the experiments incorporated a range of details and member sizes, field details that are significantly  
873 dissimilar to the tested specimens may have higher toughness demands, and thus be more fracture critical.  
874 Examples of these situations include (1) details where the extent of weld penetration or effective throat  
875 thickness is smaller (i.e. the UWR is larger) than in the tests (2) details where flanges of similar thickness are  
876 connected; in these situations, the reinforcement provided by the flared shape of the weld is absent (in contrast  
877 to the unequal flange connection where significant reinforcement is present due to the shape of the weld  
878 transition – see Figure 5 introduced previously). An accurate assessment of these factors is possible only

879 through additional testing or a comprehensive parametric study using FE simulations similar to the ones  
880 described in this paper.

881 2. A rigorous reliability analysis to determine capacity factors ( $\phi$  – factors) for design of these connections has  
882 not been conducted, neither has a strength characterization approach been developed. These are subjects of  
883 ongoing study. However, based on the performance of these details, and the insights provided by the FE  
884 simulations, a possible route for implementation of this research is the prescriptive use of details similar to the  
885 ones tested.

886 3. The toughness estimate used in the fracture mechanics analysis (i.e. 20 ft-lb) may not be conservative for  
887 columns that are exposed to low temperatures ( $\leq 50^{\circ}\text{F}$ ), since the base metal (i.e. in the core of heavy sections)  
888 toughness is required at  $70^{\circ}\text{F}$ . AISC 341-10 (2010) requires that toughness qualification tests be no more than  
889  $20^{\circ}\text{F}$  above the lowest anticipated service temperature. It is also pertinent to mention here that the 20 ft-lb at  
890  $70^{\circ}\text{F}$  toughness (in the core) is not required when the column flanges are thinner than 1.5”, since adequate  
891 toughness is expected from these. Consequently, while it is highly likely that the results of this study are  
892 applicable to these situations (Test W14C supports this), it is noted that the 20 ft-lb toughness is not explicitly  
893 required by the AISC 341-10 for these situations.

894 4. Residual stresses in welds, as well as in-situ weld toughness are sensitive to parameters of the welding  
895 procedures as well as physical constraints at the time of welding (Masubuchi, 1980). This should be considered  
896 as a factor in the generalization/implementation of results.

897 5. The demand analysis (i.e. the NTH simulations) are based on a small set of archetype buildings subjected to  
898 limited number of ground motions. While the results of this analysis are applied in a conservative manner,  
899 aspects of structural response not considered by the NTH simulation (e.g. buildings taller than 20 stories, near  
900 fault ground motions, vertical accelerations) may influence demands in the splices. Similarly, the effect of the  
901 use of high strength steel for columns on splice demands is also undetermined. As discussed previously,  
902 columns with Grade 50 material (i.e.  $F_y = 50\text{ksi}$ ) were used along with E70 welds. However, given that the  
903 columns in the NTH simulations showed very limited (or no) yielding, it may be argued that the strength of the  
904 columns may not affect demands in the splices.

905 6. Since the NTH simulations are based on planar frames, three-dimensional effects (due to bidirectional shaking)  
906 are not explicitly incorporated in this study. However, the effects of this are anticipated to be modest. Moreover,

907 it is important to recall that the NTH simulations only featured Special Moment Resisting Frames and not  
908 Intermediate Moment Frames (IMFs), which are not subject to the SCWB requirement. Thus, it may be argued  
909 that the results are not applicable to IMFs wherein the splice force/moment demands may be larger. However,  
910 two points may be made in response. First, even in the SMRFs (considered in this study) which have the SCWB  
911 requirement, the column end interaction ratio approached yield for the 20-story frame. Second, IMFs are limited  
912 to a 35' height restriction in Seismic Design Category D. The NTH results for the 4-story SMRF (which is  
913 similar in height to this limit) suggest that the response in these cases is dominated by first mode response with  
914 low demands at the splice. It is not unrealistic to extrapolate this response to IMFs.

915 7. While the effects of the above factors have not been determined, in some ways, the results of the study may also  
916 be conservative with respect to field conditions. For example, the test specimens required flipping for the  
917 application of reversed cyclic loading. Each of these “flips” required approximately 1-2 hours to execute,  
918 introducing the possibility of strain aging (Pense, 2004), and associated detrimental effects on splice  
919 performance. These effects are not present in field splices, which are subject to a higher rate of loading.

920 Thus, while the results of this study are promising from a standpoint of utilizing PJP-welded splices in seismic  
921 moment frames, some of the issues above must be addressed before their adoption. While it may not be feasible to  
922 conduct additional full-scale testing, focused parametric simulation through FE simulation may greatly aid the  
923 generalization and implementation of these results.

924

#### 925 **ACKNOWLEDGMENTS**

926 This project was funded by the American Institute of Steel Construction (AISC). Herrick Steel of Stockton,  
927 California, and Gayle Manufacturing Company of Woodland, California generously donated and fabricated steel  
928 materials for this research and their donations are gratefully acknowledged. California Erectors of Benicia,  
929 California donated their time towards welding of the specimens. The authors also thank Mr. Tom Schlafly of AISC,  
930 Bob Hazelton of Herrick Steel and Gary Glenn of Gayle Manufacturing in addition to the AISC research committee,  
931 specifically James Malley and John Barsom for providing oversight and direction to the testing plans and  
932 interpretation of results. The large scale experiments described in this report were conducted at the Network for  
933 Earthquake Engineering Simulation (NEES) equipment site at the University of California at Berkeley in Richmond,  
934 California. The authors would also acknowledge the NEES and William Vuong, undergraduate researcher from the

935 University of California at Davis, for assisting with the testing. The findings and opinions of this paper are those of  
 936 the authors and do not necessarily represent those of the major sponsor, i.e. AISC.

### 937 NOTATION

938	$CTOD_C$	:	Critical Crack Tip Opening Displacement.
939	$E, \nu$	:	Modulus of elasticity of steel (29,000 ksi), Poisson's ratio (0.3).
940	$F_y$	:	Specified yield stress.
941	$F_y^{flange}$	:	Measured yield stress of smaller column flange.
942	$IR$	:	Interaction Ratio of column section, defined as
943			$IR = \frac{P}{P_y} + \frac{8}{9} \frac{M}{M_p}$ for $\frac{P}{P_y} > 0.2$ ; $IR = \frac{P}{2P_y} + \frac{M}{M_p}$ for $\frac{P}{P_y} < 0.2$
944			Where $P_y, M_p$ is the axial force capacity and plastic moment capacity of the
945			smaller column. $P, M$ are force and moment at the splice.
946	$IR_{peak}^{median}, IR_{peak}^{max}$	:	The median and maximum (over 20 ground motions) values of the peak
947			Interaction Ratio (peak within each time history).
948	$J_I$	:	Mode-I J-integral
949	$K_I, K_{IC}$	:	Stress intensity factor demand, capacity.
950	$M_{splice}$	:	Applied moment at the splice.
951	$M_p^{smaller-section}$	:	Plastic moment capacity of the smaller cross section such that
952			$M_p^{smaller-section} = R_y F_y Z_x$ , wherein $R_y$ is the ratio of the estimated to specified
953			yield strength, and $Z_x$ is the plastic section modulus of the smaller section.
954	$M_{splice}^{max}$	:	Maximum moment observed in the splice during experiment.
955	$V_{splice}^{max}$	:	Maximum shear observed in the splice during experiment.
956	$V_y^{smaller-section}$	:	Shear strength of the smaller cross section such that
957			$V_y^{smaller-section} = 0.6 \times F_y \times A_{web}^{smaller-section}$
958	$\Delta_{peak}^{median}, \Delta_{peak}^{max}$	:	The median and maximum (over 20 ground motions) values of the peak
959			Interstory drift (peak within each time history).
960	$\sigma_{flange}$	:	Estimated stress in the tension flange based on section analysis.

## REFERENCES

- 961
- 962 ABAQUS, (2012), User's Manual, Hibbitt, Karlsson, and Sorensen, Inc., Providence, RI
- 963 AISC (2010). Seismic provisions for structural steel buildings, American Institute of Steel Construction, Inc.,  
964 Chicago, IL.
- 965 AISC. (2011). Steel construction manual, 14th Ed., American Institute of Steel Construction, Inc., Chicago, IL.
- 966 Anderson, T.L. (1995), Fracture Mechanics, 2nd Ed., CRC Press, Boca Raton, FL.
- 967 American Society of Civil Engineers (2010). Minimum Design Loads for Buildings and Other Structures, Reston,  
968 VA, USA.
- 969 AWS, (2004). Structural Welding Code – Steel. AWS D1.1/D1.1M: 2004, American Welding Society, Miami,  
970 Florida.
- 971 AWS, (2009). Structural Welding Code – Seismic Supplement. AWS D1.8/D1.8M: 2009, American Welding  
972 Society, Miami, Florida.
- 973 Barsom, J.M., and Rolfe, S.T. Fracture and Fatigue Control in Structures. ASTM Press, 1999.
- 974 Bažant, Z.P. (1984), "Size Effect in Blunt Fracture: Concrete, Rock, Metal," *Journal of Engineering Mechanics*,  
975 ASCE, 110(4), 518–535.
- 976 Bruneau, M., and Mahin, S., (1991). "Full-scale tests of Butt-Welded Splices in Heavy-Rolled Steel Sections  
977 Subjected to Primary Tensile Stresses," *Engineering Journal*, American Institute of Steel Construction,  
978 First Quarter, 1-17.
- 979 Dubina, D., and Stratan, A. (2002). "Behaviour of welded connections of moment resisted frames beam-to-column  
980 joints," *Engineering Structures*, Elsevier, 24(11), 1431-1440.
- 981 Engelhardt, M.D., Sabol, T.A. (1994). "Testing of welded steel moment connections in response to the Northridge  
982 earthquake," Research Progress Report, American Institute of Steel Construction Northridge Steel Update  
983 I, American Institute of Steel Construction, Chicago, IL
- 984 Fell, B.V., Kanvinde, A.M., Deierlein, G.G., and Myers, A.T. (2009), "Experimental Investigation of Inelastic  
985 Cyclic Buckling and Fracture of Steel Braces," *Journal of Structural Engineering*, ASCE, 135(1), 19-32.
- 986 FEMA. (2000). "FEMA-350: Recommended design criteria for new steel moment-frame buildings," Federal  
987 Emergency Management Agency, Washington, D.C.
- 988 Gomez, I.R., Kanvinde, A.M., and Deierlein, G.G., (2010), "Exposed column base connections subjected to axial  
989 compression and flexure," Report Submitted to the American Institute of Steel Construction, Chicago, IL.
- 990 Gupta, A. and Krawinkler, H., (1999). "Seismic Demands for Performance Evaluation of Steel Moment Resisting  
991 Frame Structures (SAC Task 5.4.3), Report No. 132, John A. Blume Earthquake Engineering Center,  
992 Stanford University, Stanford, CA.
- 993 Hayes, J.M., (1957). "Effects of Initial Eccentricities on Column Performance and Capacity," *Journal of the*  
994 *Structural Division*, American Society of Civil Engineers, Paper 1440.

995 Kanvinde A.M., and Deierlein G.G., (2006), "The Void Growth Model and the Stress Modified Critical Strain  
996 Model to Predict Ductile Fracture in Structural Steels" *Journal of Structural Engineering*, ASCE, 132(12),  
997 1907-1918.

998 Kanvinde A.M., Fell B.V., Gomez I.R., and Roberts M., (2008), "Predicting fracture in structural fillet welds using  
999 traditional and micromechanics-based models," *Engineering Structures*, Elsevier, 30(11), 3325-3335.

1000 Kaufman, E. and Fisher, J. (1995). "A Study of the Effects of Materials and Welding Factors on Moment Frame  
1001 Weld Joint Performance Using a Small-scale Tension Specimen," *Technical Report 95-08*, SAC Joint  
1002 Venture, Sacramento, CA, Dec. 1995.

1003 Kaufmann, E.J., Metrovich, B.R., and Pense, A.W., (2001). "Characterization of Cyclic Inelastic Strain Behavior on  
1004 Properties of A572 Gr. 50 and A913 Gr. 50 Rolled Sections," Final Report to American Institute of Steel  
1005 Construction, ATLSS Report 01-13, Lehigh University, Bethlehem, PA.

1006 Lignos, D.G., Krawinkler, H., Whittaker, A. S. (2011). "Prediction and Validation of Sidesway Collapse of Two  
1007 Scale Models of a 4-Story Steel Moment Frame," *Earthquake Engineering and Structural Dynamics*, 40  
1008 (7), 807-825.

1009 Masubuchi, K., (1980). *Analysis of Welded Structures*, Pergamon Press, 1980.

1010 Matsuishi, M. and Endo, T. (1968). "Fatigue of metals subjected to varying stress," *Japan Soc. Mech. Engineering*.

1011 McMeeking, R.M. and Parks, D.M. (1979), "On Criteria for J-Dominance of Crack-Tip Fields in Large Scale  
1012 Yielding," *Elastic-Plastic Fracture*, ASTM STP 668, J.D. Landes, J.A. Begley, and G.A. Clarke, Eds.,  
1013 American Society for Testing and Materials, pp 175-194.

1014 Myers A.T., Kanvinde, A.M., Deierlein, G.G., and Fell, B.V. (2009), "Effect of Weld Details on the Ductility of  
1015 Steel Column Baseplate Connections," *Journal of Constructional Steel Research*, Elsevier, 65(6), 1366-  
1016 1373.

1017 Nuttaysakul, N., (2000). "Finite element fracture mechanics study of partial penetration welded splices," *Engineers*  
1018 *Thesis*, Stanford University, Stanford, CA.

1019 OpenSEES (2009). "Open System for Earthquake Engineering Simulation," Pacific Earthquake Engineering Center,  
1020 Berkeley, CA.

1021 Popov, E.P., and Stephen, R.M., (1976). "Capacity of columns with splice imperfections," *Engineering Journal*,  
1022 American Institute of Steel Construction, First Quarter, 16-23.

1023 Rice, J.R. (1968), "A path independent Integral and the Approximate Analysis of Strain Concentration for Notches  
1024 and Cracks." *Journal of Applied Mechanics*, 35, 379-386.

1025 Richards, P.W., and Uang, C-M., (2006). "Testing protocol for short links in Eccentrically Braced Frames," *Journal*  
1026 *of Structural Engineering*, ASCE, 132(8), 1183-1191.

1027 SAC Joint Venture (1996). "Selected Results from the SAC Phase 1 Beam-Column Connection Pre-Test Analyses,"  
1028 *Technical Report 96-01* (1996), Sacramento, CA.

1029 Shen, J, Sabol, T., Akabas, B. and Sutchiewcharn, C., "Seismic demand of column splices in special moment  
1030 frames," *Engineering Journal*, American Institute of Steel Construction, the Fourth Quarter, 223-240.

1031 Shaw, S.M., (2013). "Seismic Performance of Partial Joint Penetration Welds in Special Moment Resisting Frames,"  
1032 Ph.D. Dissertation, University of California, Davis, CA.

1033 Somerville, P., Smith, N., Punyamurthula, S. and Sun, J. (1997), "Development of Ground Motion Time Histories  
1034 for Phase 2 of the FEMA/SAC Steel Project," SAC Background Document, Report No. SAC/BD-97/04.

1035